CP-violating phenomenology of flavor conserving two Higgs doublet models

Satoru Inoue,[1] Michael J. Ramsey-Musolf,[1,2] and Yue Zhang[2]

[1]*Amherst Center for Fundamental Interactions, Department of Physics, University of Massachusetts–Amherst, Amherst, Massachusetts 01003, USA*

[2]*California Institute of Technology, Pasadena, California 91125, USA*

(Received 28 March 2014; published 25 June 2014)

We analyze the constraints on *CP*-violating, flavor conserving two Higgs doublet models implied by measurements of Higgs boson properties at the Large Hadron Collider (LHC) and by the nonobservation of permanent electric dipole moments (EDMs) of molecules, atoms, and neutrons. We find that the LHC and EDM constraints are largely complementary, with the LHC studies constraining the mixing between the neutral *CP*-even states and the EDMs probing the effect of mixing between the *CP*-even and *CP*-odd scalars. Presently, the most stringent constraints are implied by the nonobservation of the ThO molecule EDM signal. Future improvements in the sensitivity of neutron and diamagnetic atom EDM searches could yield competitive or even more severe constraints. We analyze the quantitative impact of hadronic and nuclear theory uncertainties on the interpretation of the latter systems and conclude that these uncertainties cloud the impact of projected improvements in the corresponding experimental sensitivities.

DOI: 10.1103/PhysRevD.89.115023 PACS numbers: 12.60.Fr, 11.30.Er, 13.85.-t, 31.30.jn

I. INTRODUCTION

With the discovery of a 125 GeV boson at the Large Hadron Collider, exploration of the dynamics of electroweak symmetry breaking (EWSB) is front and center in particle physics. Although the properties of the new boson agree thus far with expectations for the Standard Model (SM) Higgs boson, it is possible that it constitutes but one state of a richer scalar sector. Perhaps the most widely studied extended scalar sector is the two-Higgs doublet model (2HDM). The collider and low-energy phenomenology of the 2HDM have been extensively analyzed over the years [1,2], while one version of this paradigm appears in an equally important scenario for physics beyond the Standard Model (BSM), the minimal supersymmetric Standard Model.

One of the more interesting features of the 2HDM is the presence of new sources of *CP* violation beyond that of the Standard Model Cabibbo-Kobayashi-Maskawa (CKM) matrix and the QCD "θ term." It is well known that BSM *CP* violation is required to account for the observed excess of matter over antimatter in the present Universe. If realized in nature, the 2HDM may provide the necessary *CP* violation and may enable the generation of the matter-antimatter asymmetry during the era of EWSB [3–5], and possibly the co-generation of both baryonic and dark matter in the Universe [6]. If so, then the 2HDM *CP* violation may have observable signatures in laboratory tests. At the energy frontier, *CP* violation correlations associated with the production and the decay of the lightest neutral scalar may be accessible at the LHC and/or a future high intensity e^+e^- collider. At the low-energy "intensity frontier," searches for the permanent electric dipole moments (EDMs) of atoms, molecules, and nucleons provide a powerful indirect probe [7–10]. Indeed, EDM searches are entering a new era of sensitivity, with the recent report by the ACME Collaboration of a ten times tighter limit on the electron EDM [11],[1] representing a harbinger of even more powerful probes in the future. Searches for the permanent EDM of the neutron are under way at a variety of laboratories around the world, with goals of 1 to 2 order of magnitude improvements in sensitivity. Similarly, experiments are under way to carry out improved and/or new searches for the EDMs of mercury, xenon, and radium, while longer term efforts to develop storage ring probes of the proton and light nuclei EDMs are being pursued [12].

With this context in mind, it is timely to investigate the present and prospective probes of *CP* violation in the 2HDM. To follow, we will report on such a study, focusing on the implications of present and prospective EDM searches while taking into account the LHC constraints on the properties of the 125 GeV boson. For concreteness, we consider a Z_2-symmetric variant of the 2HDM that evades potentially problematic flavor-changing neutral currents (FCNCs) but still allows for a new *CP* violation associated with the scalar potential, accommodates the present 125 GeV boson properties, and retains a rich phenomenology for future studies.

Under these assumptions, we explore scenarios wherein there exists only one physical *CP* violation phase associated with the scalar potential. The resulting scalar spectrum contains three neutral states that are *CP* violation

[1]The experiment actually constrains the ThO molecule response to an external electric field. In general, the ThO response is dominated by two operators, including the electron EDM and an electron-quark interaction. For the 2HDM, the electron EDM gives by far the larger contribution.

mixtures of neutral scalar and pseudoscalars and one pair of charged scalars. The scalar sector is then characterized by nine independent parameters that can be related to the parameters in the potential using the conditions for EWSB. We take these parameters to be the four scalar masses; the mixing angle α_b that governs the CP-odd admixture of the 125 GeV scalar; the combined vacuum expectation value (VEV) of the two neutral scalars, where $v = 246$ GeV; the conventional 2HDM mixing angles β and α; and a parameter ν (also defined below) that characterizes the degree to which the heavier states decouple from the low-energy effective theory, leaving the 125 GeV boson as the only accessible state. Note that $\alpha_b \to 0$ when $\delta \to 0$ and that, under our choice of the independent parameters, α_b encodes the effects of the sole physical phase in the scalar potential.

From our analysis, we find that

(i) Fits to the properties of the observed 125 GeV boson generally favor scenarios in which $\alpha \approx \beta - \pi/2$.

(ii) For fixed values of the scalar masses, null results for EDMs yield constraints in the $\sin\alpha_b$–$\tan\beta$ plane.

(iii) In general, the assumption that loops involving the lightest neutral scalar are dominant over those involving the remaining 2HDM scalar states does not hold. In the electron EDM case, for example, loops involving the heavier states may yield the largest contribution for moderate-to-large $\tan\beta$. In short, the "light Higgs effective theory" is not necessarily effective in this context.

(iv) At present, the ThO result yields the strongest constraints on the CP violation parameter space. Future EDM searches could significantly extend this reach, particularly for the type II 2HDM. An order-of-magnitude improvement in the sensitivity of the neutron and ^{199}Hg EDM searches would probe regions presently allowed by the ThO limit. A factor of 100 more sensitive neutron EDM search would go well beyond the present constraints and, in the event of a null result, would restrict $|\sin\alpha_b|$ to less than a few thousand. Successful completion of the Argonne ^{225}Ra EDM search at its design sensitivity would reach well beyond the ACME constraints—as well as the possible ten times better neutron and ^{199}Hg search for the type II case—though a 100 times more sensitive neutron EDM search would surpass the radium reach. For the type I model, the ACME constraints would survive even the future neutron, mercury, and radium experiments. Thus, a nonzero result for any of the latter searches would indicate the presence of a type II rather than a type I 2HDM.

(v) Determination of the diamagnetic atom (^{199}Hg, ^{225}Ra, etc.) and neutron EDM sensitivities is subject to considerable hadronic and nuclear many-body uncertainties. Those associated with the interpretation of the paramagnetic system (ThO) results are less significant. Consequently, the aforementioned statements about the relative sensitivities of future searches are provisional. Definitive conclusions will require substantial improvements in hadronic and nuclear many-body computations.

We organize the discussion of the analysis leading to these observations as follows. In Sec. II we analyze the general features of the Z_2-symmetric 2HDM, including the constraints of the EWSB conditions, the choice of independent parameters, and the structure of the interactions. Section III gives the relationship of the independent parameters and interactions to the observables of interest, including the Higgs boson event rates at the LHC (Sec. III A), the low-scale effective operators that ultimately induce EDMs of various light quark and lepton systems and their renormalization group evolution (Sec. III B), and the sensitivity of these systems to the effective operators and the corresponding EDM constraints (Sec. III C). Section IV gives the resulting constraints on the relevant parameter space. In particular, we call the reader's attention to Figs. 6 and 10. The former gives the present constraints from ThO, the neutron, and ^{199}Hg in the $\sin\alpha_b$–$\tan\beta$ plane, including the hadronic and nuclear theory uncertainties. The latter shows the prospective impact of future neutron, ^{199}Hg, and ^{225}Ra searches in comparison with the present ThO constraints. In this section, we also present an "anatomy" of the electron, neutron, and diamagnetic EDMs in terms of the 2HDM degrees of freedom, as well as the various low-energy effective operators. We summarize our conclusions in Sec. V. Expressions for the effective operator Wilson coefficients are given in the Appendix.

II. 2HDM FRAMEWORK

A. Scalar potential

In this work, we consider the flavor conserving 2HDM in order to avoid problematic flavor-changing neutral currents. As observed by Glashow and Weinberg (GW) [13], one may avoid tree-level FCNCs if diagonalization of the fermion mass matrices leads to flavor diagonal Yukawa interactions. One approach[2] to realizing this requirement is to impose a Z_2 symmetry on the scalar potential together with an appropriate extension to the Yukawa interactions (see below). In this scenario, however, one obtains no sources of CP violation beyond the SM CKM complex phase. Consequently, we introduce a soft Z_2-breaking term that yields nonvanishing CP violation terms in the scalar sector [17].

To that end, we choose a scalar field basis in which the two Higgs doublets $\phi_{1,2}$ are oppositely charged under the Z_2 symmetry

[2]Another approach to having 2HDM at the electroweak scale without the Z_2 symmetry is to assume minimal flavor violation, flavor alignment, or other variants. We do not discuss this possibility, but refer to [14–16] for recent phenomenological studies.

$$\phi_1 \to -\phi_1 \quad \text{and} \quad \phi_2 \to \phi_2, \tag{1}$$

though this symmetry will, in general, have a different expression in another basis obtained by the transformation $\phi_j = U_{jk}\phi'_k$. For example, taking

$$U = \frac{1}{\sqrt{2}}\begin{pmatrix} -1 & 1 \\ 1 & 1 \end{pmatrix}, \tag{2}$$

the transformation (1) corresponds to

$$\phi'_1 \leftrightarrow \phi'_2. \tag{3}$$

We then take the Higgs potential to have the form

$$\begin{aligned} V = {} & \frac{\lambda_1}{2}(\phi_1^\dagger\phi_1)^2 + \frac{\lambda_2}{2}(\phi_2^\dagger\phi_2)^2 + \lambda_3(\phi_1^\dagger\phi_1)(\phi_2^\dagger\phi_2) \\ & + \lambda_4(\phi_1^\dagger\phi_2)(\phi_2^\dagger\phi_1) + \frac{1}{2}[\lambda_5(\phi_1^\dagger\phi_2)^2 + \text{H.c.}] \\ & - \frac{1}{2}\{m_{11}^2(\phi_1^\dagger\phi_1) + [m_{12}^2(\phi_1^\dagger\phi_2) + \text{H.c.}] \\ & + m_{22}^2(\phi_2^\dagger\phi_2)\}. \end{aligned} \tag{4}$$

The complex coefficients in the potential are m_{12}^2 and λ_5. In general, the presence of the $\phi_1^\dagger\phi_2$ term, in conjunction with the Z_2-conserving quartic interactions, will induce other Z_2-breaking quartic operators at one-loop order. Simple power counting implies that the responding coefficients are finite, with the magnitude proportional to $m_{12}^2\lambda_k/(16\pi^2)$. Given the $1/16\pi^2$ suppression, we will restrict our attention to the tree-level Z_2-breaking bilinear term.

It is instructive to identify the *CP* violation complex phases that are invariant under a rephasing of the scalar fields. To that end, we perform an $\mathrm{SU}(2)_L \times \mathrm{U}(1)_Y$ transformation to a basis where the vacuum expectation value of the neutral component of ϕ_1 is real, while that associated with the neutral component of ϕ_2 is, in general, complex:

$$\begin{aligned} \phi_1 &= \begin{pmatrix} H_1^+ \\ \frac{1}{\sqrt{2}}(v_1 + H_1^0 + iA_1^0) \end{pmatrix}, \\ \phi_2 &= \begin{pmatrix} H_2^+ \\ \frac{1}{\sqrt{2}}(v_2 + H_2^0 + iA_2^0) \end{pmatrix}, \end{aligned} \tag{5}$$

where $v = \sqrt{|v_1|^2 + |v_2|^2} = 246\ \text{GeV}$, $v_1 = v_1^*$, and $v_2 = |v_2|e^{i\xi}$. It is apparent that, in general, ξ denotes the relative phase of v_2 and v_1. Under the global rephasing transformation

$$\phi_j = e^{i\theta_j}\phi'_j, \tag{6}$$

the couplings m_{12}^2 and λ_5 can be redefined to absorb the global phases

$$(m_{12}^2)' = e^{i(\theta_2-\theta_1)}m_{12}^2, \qquad \lambda'_5 = e^{2i(\theta_2-\theta_1)}\lambda_5, \tag{7}$$

so that the form of the potential is unchanged. It is then straightforward to observe that there exist two rephasing invariant complex phases:

$$\begin{aligned} \delta_1 &= \mathrm{Arg}[\lambda_5^*(m_{12}^2)^2], \\ \delta_2 &= \mathrm{Arg}[\lambda_5^*(m_{12}^2)v_1v_2^*]. \end{aligned} \tag{8}$$

For future purposes, we emphasize that the value of ξ is not invariant.

Denoting $\tan\beta = |v_2|/|v_1|$, the minimization conditions in the H_k^0 and A_k^0 directions give us the relations

$$\begin{aligned} m_{11}^2 = {} & \lambda_1 v^2\cos^2\beta + (\lambda_3+\lambda_4)v^2\sin^2\beta \\ & - \mathrm{Re}(m_{12}^2 e^{i\xi})\tan\beta + \mathrm{Re}(\lambda_5 e^{2i\xi})v^2\sin^2\beta, \end{aligned} \tag{9}$$

$$\begin{aligned} m_{22}^2 = {} & \lambda_2 v^2\sin^2\beta + (\lambda_3+\lambda_4)v^2\cos^2\beta \\ & - \mathrm{Re}(m_{12}^2 e^{i\xi})\cot\beta + \mathrm{Re}(\lambda_5 e^{2i\xi})v^2\cos^2\beta, \end{aligned} \tag{10}$$

$$\mathrm{Im}(m_{12}^2 e^{i\xi}) = v^2\sin\beta\cos\beta\,\mathrm{Im}(\lambda_5 e^{2i\xi}). \tag{11}$$

From the last equation, it is clear that the phase ξ can be solved for given the complex parameters m_{12}^2 and λ_5. It is useful, however, to express this condition in terms of the δ_k:

$$|m_{12}^2|\sin(\delta_2 - \delta_1) = |\lambda_5 v_1 v_2|\sin(2\delta_2 - \delta_1). \tag{12}$$

With the limit that the δ_k are small but nonvanishing, which will be appropriate for our later phenomenological discussion, Eq. (12) then implies

$$\delta_2 \approx \frac{1 - |\frac{\lambda_5 v_1 v_2}{m_{12}^2}|}{1 - 2|\frac{\lambda_5 v_1 v_2}{m_{12}^2}|}\delta_1, \tag{13}$$

so that there exists only one independent *CP* violation phase in the theory after EWSB.

A special case arises when $\delta_1 = 0$. In this case, Eq. (12) implies that

$$|m_{12}^2|\sin(\delta_2) = |\lambda_5 v_1 v_2|\sin(2\delta_2) \tag{14}$$

or

$$\cos\delta_2 = \frac{1}{2}\left|\frac{m_{12}^2}{\lambda_5 v_1 v_2}\right|. \tag{15}$$

When the right-hand side is less than 1, δ_2 has two solutions of equal magnitude and opposite sign, corresponding to the presence of spontaneous *CP* violation [18,19]:

$$\delta_2 = \pm\arccos\left(\frac{1}{2}\left|\frac{m_{12}^2}{\lambda_5 v_1 v_2}\right|\right) = \pm\left(\frac{1}{2}\left|\frac{m_{12}^2}{\lambda_5 v^2\cos\beta\sin\beta}\right|\right). \tag{16}$$

To the extent that the vacuums associated with the two opposite sign solutions are degenerate, one would expect the existence of cosmological domains [20] associated with these two vacuums. Persistence of the corresponding domain walls to late cosmic times is inconsistent with the observed homogeneity of the structure and isotropy of the cosmic microwave background. Consequently, parameter choices leading to $\delta_1 = 0$ but $\delta_2 \neq 0$ should be avoided. In practice, we will scan over model parameters when analyzing the EDM and LHC constraints. As a check, we have performed a scan with 10^6 points and find less than ten that give $\delta_1 = 0$. Thus, we are confident that the general features of our phenomenological analysis are consistent with the absence of problematic spontaneous CP violation domains.

Henceforth, for simplicity, we utilize the rephasing invariance of the δ_k and work in a basis where $\xi = 0$. In this basis, the phases of m_{12}^2 and λ_5 are redefined and related by Eq. (11). As we discuss below, we will trade the resulting dependence of observables on δ_1 [and δ_2 via δ_1 in Eq. (13)] for one independent angle in the transformation that diagonalizes the neutral scalar mass matrix.

B. Scalar spectrum

After EWSB, the diagonalization of the 2×2 charged Higgs mass matrix yields the physical charged scalar and Goldstone modes

$$H^+ = -\sin\beta H_1^+ + \cos\beta H_2^+,$$
$$G^+ = \cos\beta H_1^+ + \sin\beta H_2^+. \tag{17}$$

The charged scalar has a mass

$$m_{H^+}^2 = \frac{1}{2}(2\nu - \lambda_4 - \mathrm{Re}\lambda_5)v^2,$$
$$\nu \equiv \frac{\mathrm{Re}m_{12}^2 \csc\beta \sec\beta}{2v^2}. \tag{18}$$

For the neutral Higgs sector, the mixing between CP odd components yields the Goldstone G^0 and an orthogonal combination A^0, where

$$A^0 = -\sin\beta A_1^0 + \cos\beta A_2^0,$$
$$G^0 = \cos\beta A_1^0 + \sin\beta A_2^0. \tag{19}$$

In the presence of an explicit CP violation, A^0 is not yet a mass eigenstate. It will further mix with the CP even eigenstates H_1^0, H_2^0. The 3×3 neutral mass matrix in the basis of $\{H_1^0, H_2^0, A^0\}$ is

$$\mathcal{M}^2 = v^2 \begin{pmatrix} \lambda_1 c_\beta^2 + \nu s_\beta^2 & (\lambda_{345} - \nu)c_\beta s_\beta & -\frac{1}{2}\mathrm{Im}\lambda_5 s_\beta \\ (\lambda_{345} - \nu)c_\beta s_\beta & \lambda_2 s_\beta^2 + \nu c_\beta^2 & -\frac{1}{2}\mathrm{Im}\lambda_5 c_\beta \\ -\frac{1}{2}\mathrm{Im}\lambda_5 s_\beta & -\frac{1}{2}\mathrm{Im}\lambda_5 c_\beta & -\mathrm{Re}\lambda_5 + \nu \end{pmatrix}, \tag{20}$$

where $\lambda_{345} = \lambda_3 + \lambda_4 + \mathrm{Re}\lambda_5$. We define an orthogonal rotation matrix R to diagonalize the above mass matrix, with $R\mathcal{M}^2 R^{\mathrm{T}} = \mathrm{diag}(m_{h_1}^2, m_{h_2}^2, m_{h_3}^2)$. Generally, the matrix R can be parametrized as [21,22]

$$R = R_{23}(\alpha_c)R_{13}(\alpha_b)R_{12}(\alpha + \pi/2)$$
$$= \begin{pmatrix} -s_\alpha c_{\alpha_b} & c_\alpha c_{\alpha_b} & s_{\alpha_b} \\ s_\alpha s_{\alpha_b} s_{\alpha_c} - c_\alpha c_{\alpha_c} & -s_\alpha c_{\alpha_c} - c_\alpha s_{\alpha_b} s_{\alpha_c} & c_{\alpha_b} s_{\alpha_c} \\ s_\alpha s_{\alpha_b} c_{\alpha_c} + c_\alpha s_{\alpha_c} & s_\alpha s_{\alpha_c} - c_\alpha s_{\alpha_b} c_{\alpha_c} & c_{\alpha_b} c_{\alpha_c} \end{pmatrix}. \tag{21}$$

Both α_b and α_c are CP-violating mixing angles in the Higgs sector that depend implicitly on δ_1. In this convention, the significance of the α and β angles are the same as in the minimal supersymmetric Standard Model, and the interactions with quarks of the lightest Higgs state, h_1, depends only on one CP-violating angle α_b. The mass and CP eigenstates are related via $(H_1^0, H_2^0, A^0) = (h_1, h_2, h_3)R$. As we discuss below, α_c is determined once α_b, α, β, and the neutral scalar masses are specified. Thus, we will utilize α_b rather than δ_1 to characterize the effects of CP violation on the potential.

C. Interactions

For phenomenological analysis, we are interested in interactions of the scalar sector with the other SM particles. After EWSB, the couplings of the neutral scalars with fermions and gauge bosons can be parametrized generally as [23]

$$\mathcal{L} = -\frac{m_f}{v} h_i (c_{f,i}\bar{f}f + \tilde{c}_{f,i}\bar{f}i\gamma_5 f) + a_i h_i \left(\frac{2m_W^2}{v} W_\mu W^\mu + \frac{m_Z^2}{v} Z_\mu Z^\mu\right), \tag{22}$$

where $i = 1, 2, 3$ and where we have allowed for only flavor diagonal couplings. To arrive at the couplings, we extend the Z_2 symmetry of the scalar potential by making the following assignments to the fermions:

$$Q_L \to Q_L \quad u_R \to u_R \quad d_R \to d_R \quad \text{type I}, \tag{23}$$

$$Q_L \to Q_L \quad u_R \to u_R \quad d_R \to -d_R \quad \text{type II}. \tag{24}$$

One may make similar assignments for the leptons. The resulting Yukawa interactions before EWSB are

$$\mathcal{L}_{\mathrm{I}} = -Y_U \bar{Q}_L (i\tau_2)\phi_2^* u_R - Y_D \bar{Q}_L \phi_2 d_R + \mathrm{H.c.}, \tag{25}$$

$$\mathcal{L}_{\mathrm{II}} = -Y_U \bar{Q}_L (i\tau_2)\phi_2^* u_R - Y_D \bar{Q}_L \phi_1 d_R + \mathrm{H.c.} \tag{26}$$

Note that $\mathcal{L}_{I,II}$ satisfy the GW criterion for the absence of tree-level FCNCs.

For each of the two types of models, we solve for c_f, $\tilde{c}_f$, and a in terms of β and the orthogonal matrix R,

$$\begin{array}{lccccc} & c_{t,i} & c_{b,i} & \tilde{c}_{t,i} & \tilde{c}_{b,i} & a_i \\ \text{Type I} & R_{i2}/\sin\beta & R_{i2}/\sin\beta & -R_{i3}\cot\beta & R_{i3}\cot\beta & R_{i2}\sin\beta + R_{i1}\cos\beta\,, \\ \text{Type II} & R_{i2}/\sin\beta & R_{i1}/\cos\beta & -R_{i3}\cot\beta & -R_{i3}\tan\beta & R_{i2}\sin\beta + R_{i1}\cos\beta \end{array} \tag{27}$$

where all the up (down) type fermions have the same universal rescaled couplings as the top (bottom) quark apart from the overall factor of the quark mass.

The charged Higgs-fermion interactions are, respectively,

$$\mathcal{L}_{\bar{f}f'H^\pm} = \begin{cases} V_{ij}\cot\beta\bar{u}_i[m_{u_i}(1-\gamma_5) + m_{d_j}(1+\gamma_5)]d_jH^+ + \text{H.c.} & \text{type I} \\ V_{ij}\bar{u}_i[m_{u_i}\cot\beta(1-\gamma_5) - m_{d_j}\tan\beta(1+\gamma_5)]d_jH^+ + \text{H.c.} & \text{type II,} \end{cases} \tag{28}$$

where V stands for the CKM matrix for quark mixings.

The trilinear interactions between charged and neutral scalars, relevant for the scalar sector contribution to EDMs, are of the form

$$\mathcal{L}_{H^\pm} = -\bar{\lambda}_i v h_i H^+H^-, \tag{29}$$

where h_i and $H^\pm$ are mass eigenstates, and

$$\begin{aligned}\bar{\lambda}_i = {} & R_{i1}\cdot(\lambda_3\cos^2\beta + (\lambda_1-\lambda_4-\text{Re}\lambda_5)\sin^2\beta)\cos\beta \\ & + R_{i2}\cdot(\lambda_3\sin^2\beta + (\lambda_2-\lambda_4-\text{Re}\lambda_5)\cos^2\beta)\sin\beta \\ & + R_{i3}\cdot\text{Im}\lambda_5\sin\beta\cos\beta. \end{aligned} \tag{30}$$

We do not write down the corresponding quartic terms, as they are not needed for our phenomenological analysis.

D. Phenomenological parameters

From the Higgs potential in Eq. (4), it is possible to solve for the Higgs doublet VEVs, as well as the scalar masses and mixing angles, which are more directly related to observation. Since the aim of this work is to arrive at the phenomenological constraints on the parameter space of 2HDM, it is useful to translate these constraints into those on phenomenologically relevant parameters. The latter set includes the masses, the mixing angles, and the parameter ν introduced in Eq. (18) (whose significance we discuss below). The following table summarizes two sets of parameters (all real):

$$\begin{array}{ll} \text{Potential parameters} & \text{Phenomenological parameters} \\ \lambda_1,\lambda_2,\lambda_3,\lambda_4,\text{Re}\lambda_5,\text{Im}\lambda_5 & v,\tan\beta,\nu,\alpha,\alpha_b,\alpha_c \\ m_{11}^2,m_{22}^2,\text{Re}m_{12}^2,\text{Im}m_{12}^2 & m_{h_1},m_{h_2},m_{h_3},m_{H^+} \end{array} \tag{31}$$

Each set has 10 parameters, and it would appear to be possible to solve one set of parameters from the other. However, the minimization conditions for the A_k^0 in Eq. (11) imply that there exists only one independent CP violation phase and hence that the CP violation mixing angles α_b and α_c are not independent. As we show below, one may solve for α_c (α_b) in terms of α_b (α_c), the physical neutral scalar masses α and β.

Two additional remarks are in order. First, the phenomenological significance of the parameter ν is that it controls the mass scale of the second Higgs doublet. In the decoupling limit wherein one reverts to the SM, one has $\nu \gg 1$. Equations (18) and (20) then imply that $H^\pm$, $h_3 \approx A^0$, and the linear combination $h_2 \approx \sin\beta H_1^0 - \cos\beta H_2^0$ also decouple with an approximately common mass ν. The resulting low-energy theory contains only one CP even scalar h_1, which is the SM Higgs boson. In the same decoupling limit, we also have $\alpha_{b,c} \to 0$ and $\alpha \to \beta - \pi/2$. Away from the decoupling limit, both doublets are at the electroweak scale, and we have to treat ν as an independent input parameter.

Second, it is useful to consider the CP conserving limit, with a real Higgs potential, i.e., $\text{Im}\lambda_5 = 0$ and $\text{Im}m_{12}^2 = 0$. Absent spontaneous CP violation, $\xi = 0$ and the matrix (20) is block diagonalized with vanishing $\mathcal{M}_{13}^2$ and $\mathcal{M}_{23}^2$ elements. In this regime, one has $\alpha_b = \alpha_c = 0$, and the independent parameters become

$$\begin{array}{ll} \text{Potential parameters} & \text{Phenomenological parameters (no } CP \text{ violation)} \\ \lambda_1,\lambda_2,\lambda_3,\lambda_4,\lambda_5 & v,\tan\beta,\alpha \\ m_{11}^2,m_{22}^2,m_{12}^2 & m_{h_1},m_{h_2},m_{h_3},m_{H^+} \end{array}\,. \tag{32}$$

Although there exist eight potential parameters in this case, the condition of no spontaneous CP violation reduces the number of independent parameters to seven, which one may choose to be those displayed in the right-hand column of the table.

For the general scenario that allows for CP violation, it is useful to record the relationships between the phenomenological parameters and those in the potential:

$$\tan\beta = \frac{(m_{h_2}^2 - m_{h_3}^2)\cos\alpha_c \sin\alpha_c + (m_{h_1}^2 - m_{h_2}^2\sin^2\alpha_c - m_{h_3}^2\cos^2\alpha_c)\tan\alpha\sin\alpha_b}{(m_{h_2}^2 - m_{h_3}^2)\tan\alpha\cos\alpha_c\sin\alpha_c - (m_{h_1}^2 - m_{h_2}^2\sin^2\alpha_c - m_{h_3}^2\cos^2\alpha_c)\sin\alpha_b}, \tag{33}$$

$$\lambda_1 = \frac{m_{h_1}^2\sin^2\alpha\cos^2\alpha_b + m_{h_2}^2 R_{21}^2 + m_{h_3}^2 R_{31}^2}{v^2\cos\beta^2} - \nu\tan^2\beta, \tag{34}$$

$$\lambda_2 = \frac{m_{h_1}^2\cos^2\alpha\cos^2\alpha_b + m_{h_2}^2 R_{22}^2 + m_{h_3}^2 R_{32}^2}{v^2\sin\beta^2} - \nu\cot^2\beta, \tag{35}$$

$$\mathrm{Re}\lambda_5 = \nu - \frac{m_{h_1}^2\sin^2\alpha_b + \cos^2\alpha_b(m_{h_2}^2\sin^2\alpha_c + m_{h_3}^2\cos^2\alpha_c)}{v^2}, \tag{36}$$

$$\lambda_4 = 2\nu - \mathrm{Re}\lambda_5 - \frac{2m_{H^+}^2}{v^2}, \tag{37}$$

$$\lambda_3 = \nu - \frac{m_{h_1}^2\sin\alpha\cos\alpha\cos^2\alpha_b - m_{h_2}^2 R_{21}R_{22} - m_{h_3}^2 R_{31}R_{32}}{v^2\sin\beta\cos\beta} - \lambda_4 - \mathrm{Re}\lambda_5, \tag{38}$$

$$\mathrm{Im}\lambda_5 = \frac{2\cos\alpha_b[(m_{h_2}^2 - m_{h_3}^2)\cos\alpha\sin\alpha_c\cos\alpha_c + (m_{h_1}^2 - m_{h_2}^2\sin^2\alpha_c - m_{h_3}^2\cos^2\alpha_c)^2\sin\alpha\sin\alpha_b]}{v^2\sin\beta}. \tag{39}$$

Note that Eq. (33) implies that α_b, α_c, α, β, and the neutral scalar masses are not all independent, as advertised. The remaining equations (34)–(39), together with the minimization conditions (9)–(11), can be used to solve for the nine independent phenomenological parameters in Eq. (31).

In order to make the presence of only one independent CP violation phase apparent, we chose to eliminate one of the two CP violation mixing angles (α_c) in terms of the other parameters, including the other CP violation mixing angle (α_b) that vanishes in the CP-conserving 2HDM and the remaining parameters that survive in the absence of a CP violation.

1. Parameter ranges

Theoretical constraints on the parameter space follow from requirements of the stability of the electroweak vacuum and perturbativity [18]. While the latter is not an absolute requirement for the validity of the theory, our phenomenological study relies on perturbative computations of observables, so we restrict our attention to the domain of naive perturbativity, expressed in terms of the quartic couplings

$$0 < \lambda_1 < 4\pi, \qquad 0 < \lambda_2 < 4\pi,$$
$$\lambda_3 > -\sqrt{\lambda_1\lambda_2}, \qquad \lambda_3 + \lambda_4 - |\lambda_5| > -\sqrt{\lambda_1\lambda_2}. \tag{40}$$

Using Eqs. (34)–(39), we translate these conditions into constraints on the phenomenological parameters. To illustrate, we take h_1 to be the 125 GeV Higgs boson discovered at the LHC. For the ranges of other parameters, we allow m_{h_2}, $m_{h_3} \in [125, 500]$ GeV and α, $\alpha_b \in [-\pi/2, \pi/2]$ (notice α_c is not independent, as discussed above). The resulting region, consistent with the conditions (40) in the $\nu - \tan\beta$ plane, is shown in Fig. 1.

As discussed in the fit to LHC Higgs data in Sec. III A below—especially in the type II 2HDM—the fit to the LHC data on the Higgs boson production and decay rates points to a strong correlation between the angles α and β, with $\alpha \approx \beta - \pi/2$ (see Fig. 2). If this is taken to be a constraint, we can further reduce the set of phenomenological input parameters to

$$\alpha_b, \quad \tan\beta, \quad m_{H^+}, \quad m_{h_1}, \quad m_{h_2}, \quad m_{h_3}, \quad \nu. \tag{41}$$

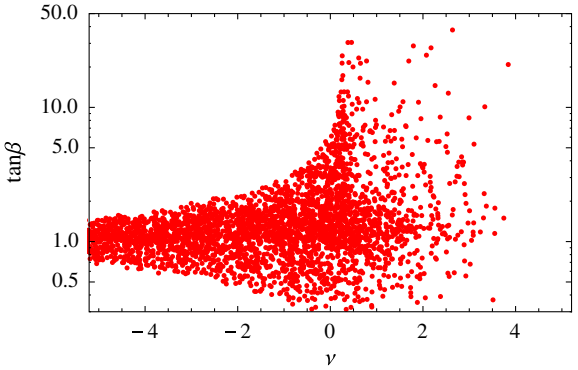

FIG. 1 (color online). Theoretical constraints on the $\nu - \tan\beta$ parameter space.

When either of the *CP* violation mixing angles α_b or α_c is fixed, the other can be obtained from Eq. (33),

$$\alpha_b = \arcsin\left[\frac{(m_{h_2}^2 - m_{h_3}^2)\sin 2\alpha_c \tan 2\beta}{2(m_{h_1}^2 - m_{h_2}^2 \sin^2\alpha_c - m_{h_3}^2 \cos^2\alpha_c)}\right], \tag{42}$$

or, alternatively,

$$\alpha_c^{\pm} = \arctan\left[\frac{(m_2^2 - m_3^2)\tan 2\beta \pm \sqrt{(m_2^2 - m_3^2)^2 \tan^2 2\beta - 4\sin^2\alpha_b (m_1^2 - m_2^2)(m_1^2 - m_3^2)}}{2(m_1^2 - m_2^2)\sin\alpha_b}\right]. \tag{43}$$

For a given α_b, there are two solutions for α_c. We find that they satisfy the relation $\tan\alpha_c^+ \tan\alpha_c^- = (m_{h_1}^2 - m_{h_3}^2)/(m_{h_1}^2 - m_{h_2}^2)$, which is approximately 1, in the limit $m_{h_1} \ll m_{h_2} \approx m_{h_3}$. Figure 2 illustrates the above relations between α_b and α_c for a set of sample parameters. One can see on the right panel that the expression for $\alpha_c^{\pm}$ contains a discontinuity at $\tan\beta = 0$ (for fixed color, blue or magenta). For our phenomenological studies, we choose α_c^+ for $\tan\beta < 1$ and α_c^- for $\tan\beta > 1$ in order to avoid this discontinuity. Physically, our choice corresponds to h_3 being mostly *CP* odd; α_c^- for $\tan\beta < 1$ and α_c^+ for $\tan\beta > 1$ correspond to the case where h_2 is mostly *CP* odd. We have observed that the choice between α_c^+ and α_c^- does not make a qualitative difference in the conclusions discussed below.

III. OBSERVABLES

A. Event rates of all Higgs decay channels at LHC

In this work, we assume the light neutral scalar from the 2HDM is the 125 GeV Higgs boson discovered at the LHC. In the presence of the *CP* violation interactions in Eq. (22), the Higgs production and decay rates are modified as follows:

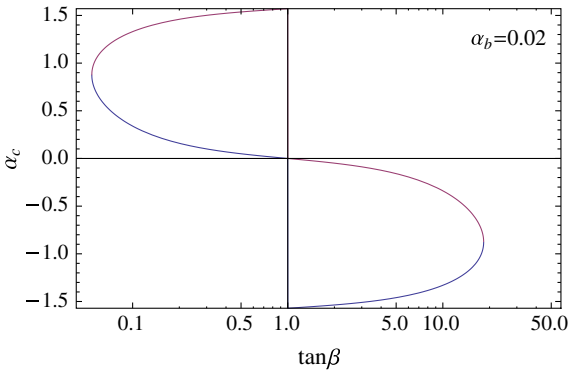

FIG. 2 (color online). Solutions for α_c^+ (blue) and α_c^- (magenta) as a function of $\tan\beta$ using Eq. (43) for fixed $\alpha_b = 0.02$. The other parameters are $m_{H^+} = 420$ GeV, $m_{h_2} = 400$ GeV, $m_{h_3} = 450$ GeV, and $\nu = 1.0$.

$$\frac{\sigma_{gg\to h_1}}{\sigma_{gg\to h_1}^{\rm SM}} = \frac{\Gamma_{h_1\to gg}}{\Gamma_{h\to gg}^{\rm SM}} \approx \frac{(1.03c_t - 0.06c_b)^2 + (1.57\tilde{c}_t - 0.06\tilde{c}_b)^2}{(1.03 - 0.06)^2}, \tag{44}$$

$$\frac{\Gamma_{h_1\to\gamma\gamma}}{\Gamma_{h\to\gamma\gamma}^{\rm SM}} \approx \frac{(0.23c_t - 1.04a)^2 + (0.35\tilde{c}_t)^2}{(0.23 - 1.04)^2}, \tag{45}$$

$$\frac{\sigma_{VV\to h_1}}{\sigma_{VV\to h}^{\rm SM}} = \frac{\sigma_{V^*\to Vh_1}}{\sigma_{V^*\to Vh}^{\rm SM}} = \frac{\Gamma_{h_1\to WW}}{\Gamma_{h\to WW}^{\rm SM}} = \frac{\Gamma_{h_1\to ZZ}}{\Gamma_{h\to ZZ}^{\rm SM}} = a^2, \tag{46}$$

$$\frac{\Gamma_{h_1\to b\bar{b}}}{\Gamma_{h\to b\bar{b}}^{\rm SM}} = \frac{\Gamma_{h_1\to\tau^+\tau^-}}{\Gamma_{h\to\tau^+\tau^-}^{\rm SM}} \approx c_b^2 + \tilde{c}_b^2. \tag{47}$$

The modified event rates will be constrained by the inclusive data in Higgs decay channels, which are summarized in Table I. Since we are interested only in the couplings of h_1, all of the above couplings (a, c_f, and $\tilde{c}_f$) can be expressed in terms of only three parameters—β, α, and α_b—where α_b is the *CP* violation mixing angle. In the presence of a *CP* violation, the global fit to the combined results measured by the ATLAS [24] and CMS [25] collaborations have been performed in several previous works [4,26–29]. In this work, we follow the same parametrization as [4] and present the results for both type I and type II 2HDMs.

B. T- and P-violating effective operators, RG running and matching

We now turn to the low-energy sector, focusing on the EDMs of the neutron, neutral atoms, and molecules[3] that presently yield the most stringent constraints on a flavor diagonal *CP* violation. The relevant time-reversal-and-parity-violating (TVPV) effective operators for our study are the elementary fermion EDMs, the quark chromo EDMs (CEDM), and the Weinberg three gluon (or gluon CEDM) operators. The corresponding effective Lagrangian valid below the electroweak scale is

[3]Technically speaking, the paramagnetic molecule response to the external field.

TABLE I. LHC data on all measured Higgs decay channels from the ATLAS and CMS collaborations.

	$\gamma\gamma$	WW	ZZ	Vbb	$\tau\tau$
ATLAS	1.6 ± 0.3	1.0 ± 0.3	1.5 ± 0.4	-0.4 ± 1.0	0.8 ± 0.7
CMS	0.8 ± 0.3	0.8 ± 0.2	0.9 ± 0.2	1.3 ± 0.6	1.1 ± 0.4

$$\begin{aligned}\mathcal{L}_{\rm eff} &= -i\sum_f \frac{d_f}{2}\bar{f}\sigma_{\mu\nu}\gamma_5 f F^{\mu\nu} \\ &\quad - i\sum_q \frac{\tilde{d}_q}{2}\bar{q}\sigma_{\mu\nu}\gamma_5 T^a q G^{a\mu\nu} \\ &\quad + \frac{d_w}{6} f^{abc}\epsilon^{\mu\nu\rho\sigma} G^a_{\mu\lambda} G^{b\lambda}_{\nu} G^c_{\rho\sigma} \qquad (48)\\ &\equiv i\sum_f \frac{\delta_f}{\Lambda^2} m_f e \bar{f}\sigma_{\mu\nu}\gamma_5 f F^{\mu\nu} \\ &\quad + i\sum_q \frac{\tilde{\delta}_q}{\Lambda^2} m_q g_s \bar{q}\sigma_{\mu\nu}\gamma_5 T^a q G^{a\mu\nu} \\ &\quad + \frac{C_{\tilde{G}}}{2\Lambda^2} g_s f^{abc}\epsilon^{\mu\nu\rho\sigma} G^a_{\mu\lambda} G^{b\lambda}_{\nu} G^c_{\rho\sigma}, \qquad (49)\end{aligned}$$

where we take the convention $\epsilon^{0123} = +1$. In the first line, we have expressed the effective operators in terms of dimensional coefficients, while in the second we have followed Ref. [7] and rewritten the operators in terms of the dimensionless quantities δ_f, $\tilde{\delta}_q$, and $C_{\tilde{G}}$; the scale of physics beyond the Standard Model Λ; and the fermion masses. Doing so is consistent with the approach of a low-energy effective field theory, wherein one makes the relevant scales and their hierarchy explicit. On general grounds, one then expects the remaining dimensionless Wilson coefficients to be comparable in magnitude, all other considerations being equal. We note that in the versions of the 2HDM considered here, the dipole operators for a given fermion are naturally proportional to its Yukawa coupling, though in other BSM scenarios they need not necessarily be. Consequently, it is appropriate to scale out the fermion masses. The dimensionless EDM, δ_q, the quark CEDM, $\tilde{\delta}_q$, and the gluon CEDM are related to the usual definitions by [7]

$$\begin{aligned}\delta_f &\equiv -\frac{\Lambda^2 d_f^{\gamma}}{2eQ_q m_q}, \qquad \tilde{\delta}_q \equiv -\frac{\Lambda^2 d_q^G}{2m_q}, \\ C_{\tilde{G}} &= \frac{\Lambda^2 d_w}{3g_s}. \qquad (50)\end{aligned}$$

Henceforth, we set $\Lambda = v$. The dominant contributions to these coefficients arise at two-loop level at the 2HDM scale $\Lambda \sim v$ and have been summarized in Appendix A.

We also take account of the TVPV four-quark operators that have an impact on the renormalization group (RG) running. They arise in the 2HDM model at tree level from a neutral Higgs exchange, as shown in Fig. 3. We are particularly interested in the operators containing the bottom quark, whose coefficients are enhanced when $\tan\beta$ is large, thereby making a significant contribution in certain cases. Those involving only light quarks are suppressed by products of their small Yukawa couplings and are, therefore, neglected here. The operators under consideration are

$$\begin{aligned}\mathcal{L}^{4q}_{\rm eff} &= \frac{C_4^b}{\Lambda^2}(\bar{b}b)(\bar{b}i\gamma_5 b) + \frac{\tilde{C}_1^{bq}}{\Lambda^2}(\bar{b}b)(\bar{q}i\gamma_5 q) \\ &\quad + \frac{\tilde{C}_1^{qb}}{\Lambda^2}(\bar{q}q)(\bar{b}i\gamma_5 b), \qquad (51)\end{aligned}$$

where $q = u,\ d$. At the 2HDM scale $\Lambda = v$, these coefficients are

$$\begin{aligned}C_4^b(\Lambda) &= \sum_i \frac{m_b^2}{m_{h_i}^2} c_{b,i}\tilde{c}_{q,i}, \\ \tilde{C}_1^{bq}(\Lambda) &= \sum_i \frac{m_b m_q}{m_{h_i}^2} \tilde{c}_{b,i} c_{q,i}, \\ \tilde{C}_1^{qb}(\Lambda) &= \sum_i \frac{m_b m_q}{m_{h_i}^2} c_{b,i}\tilde{c}_{b,i}. \qquad (52)\end{aligned}$$

In order to calculate the neutron and atomic EDMs, we account for the renormalization group running effect of the one-loop QCD corrections. The Wilson coefficients in Eq. (49) are evolved from Λ down to the GeV scale, based on the RG equations (RGE) [30–32]

$$\frac{d}{d\ln\mu}\left(\frac{\delta_q}{Q_q}, \tilde{\delta}_q, -\frac{3C_{\tilde{G}}}{2}\right) = \left(\frac{\delta_q}{Q_q}, \tilde{\delta}_q, -\frac{3C_{\tilde{G}}}{2}\right)\cdot\frac{\alpha_S}{4\pi}\begin{pmatrix} 8C_F & 0 & 0 \\ -8C_F & 16C_F - 4N & 0 \\ 0 & 2N & N + 2n_f + \beta_0 \end{pmatrix}, \qquad (53)$$

where $q = u,\ d,\ b,\ N = 3,\ C_F = (N^2-1)/(2N) = 4/3$, and $\beta_0 = (11N - 2n_f)/3$.

Between the 2HDM scale Λ and m_b, we use the $n_f = 5$ version of the above RGE. In addition, there are contributions through mixing from the four-quark operators in Eq. (51). In particular, the coefficient C_4^b mixes with—and contributes to thee b-quark CEDM and captures the leading logarithmic terms of the one-loop result [33]. The

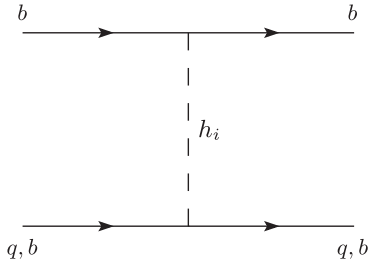

FIG. 3. Tree-level contribution to the P- and T-odd four-quark operators.

coefficients $\tilde{C}_1^{bq}$ and $\tilde{C}_1^{qb}$ also contribute to the light quark CEDM through RGE operator mixing, as discussed in detail in [31]. This reproduces the leading logarithmic terms in the Barr-Zee type contribution to the CEDM with a b quark in the upper loop. In this calculation, we keep only the leading logarithmic terms that make additional contributions to the CEDMs of bottom and light quarks at the matching scale $\mu = m_b$:

$$\Delta\tilde{\delta}_b(m_b) \approx \frac{1}{8\pi^2} C_4^b(\Lambda) \log\frac{\Lambda}{m_b}, \tag{54}$$

$$\Delta\tilde{\delta}_q(m_b) \approx \frac{g_s^2}{64\pi^4}\frac{m_b}{m_q}(\tilde{C}_1^{bq} + \tilde{C}_1^{qb})\left(\log\frac{\Lambda}{m_b}\right)^2. \tag{55}$$

At the same scale, the bottom quark is integrated out and its CEDM makes a shift to the Weinberg operator [31,34]

$$\Delta C_{\tilde{G}}(m_b) = \frac{\alpha_S(m_b)}{12\pi}\tilde{\delta}_b(m_b), \tag{56}$$

where the b-quark CEDM $\tilde{\delta}_b(m_b)$ at the m_b scale includes both the top quark contribution Eq. (A2), which evolves under the RGE, and the shift (54).

After taking these renormalization effects, the coefficients δ_q, $\tilde{\delta}_q^G$, and $C_{\tilde{G}}$ are further evolved down to the GeV scale according to RGE with 4 or 3 flavors, for the interval above or below the charm quark mass scale, respectively.

C. Current and future EDM constraints

We now analyze the constraints implied by null EDM search results by considering, in turn, paramagnetic atoms and molecules, the neutron, and diamagnetic atoms. Within the context of the flavor conserving 2HDMs, constraints from the paramagnetic systems translate into limits on the electron EDM (d_e), while in a model-independent analysis, paramagnetic results bound a linear combination of d_e and a dimension-six semileptonic interaction. The neutron EDM (d_n) is sensitive primarily to the quark EDM and CEDMs, as well as the *CP* violation three-gluon operator, while the *CP* violation four-(light)quark operator contributions are subdominant in the 2HDM context. For the diamagnetic systems, such as ^{199}Hg, the quark EDM contribution is, in general, relatively suppressed, as is a dimension-six semileptonic tensor interaction that can be more important in contexts apart from the 2HDM. Thus, the quark CEDM and three-gluon operators are the most significant for the diamagnetic systems in the 2HDM.

1. Electron EDM

Currently, the electron EDM is most strongly constrained by the ACME experiment [11], which searched for an energy shift of ThO molecules due to an external electric field. The external field induces the spin of the unpaired electron to lie along the intermolecular axis, sampling the large internal electric field associated with the polar molecule. The measured energy shift is also sensitive to the TVPV electron-nucleon interaction

$$\mathcal{L}_{eN}^{\text{eff}} = -\frac{G_F}{\sqrt{2}} C_S^{(0)} \bar{e} i\gamma_5 e \bar{N} N + \cdots, \tag{57}$$

where the "$+\cdots$" denotes subleading semileptonic interactions and the leading term arises from the four fermion operators [7]

$$[\text{Im}C_{ledq}(\bar{e}i\gamma_5 e)(\bar{d}d) - \text{Im}C_{lequ}^{(1)}(\bar{e}i\gamma_5 e)(\bar{u}u)]/(2v^2). \tag{58}$$

In the 2HDMs considered in this work, these four-fermion operators are obtained by integrating out the neutral Higgs bosons at tree level,

$$\begin{aligned} C_S^{(0)} &= -g_s^{(0)}(\text{Im}C_{ledq} - \text{Im}C_{lequ}^{(1)}) \\ &= -2g_s^{(0)}\sum_{i=1}^{3}\frac{m_e}{m_{h_i}^2}(m_d\tilde{c}_{e,i}c_{d,i} + m_u\tilde{c}_{e,i}c_{u,i}), \end{aligned} \tag{59}$$

where $g_s^{(0)}$ is the isoscalar nucleon scalar density form factor at zero momentum transfer (also known as the "σ term"). The ACME experiment gives the constraint [11]

$$|\mathcal{E}_{\text{eff}} d_e + W_S C_S^{(0)}| < 7.0 \times 10^{-18}\ \text{eV}, \tag{60}$$

where the effective field experienced by the unpaired electron is $\mathcal{E}_{\text{eff}} = 84\ \text{GV/cm}$ and $W_S = 1.2 \times 10^{-9}$ eV. Since $C_S^{(0)}$ is proportional to the product of the electron mass m_e and light quark masses $m_{u,d}$, one may safely neglect the semileptonic interaction and translate Eq. (60) into a bound on d_e or, equivalently, δ_e.

2. Neutron EDM

The dependence of the neutron EDM on the leading nonleptonic *CP* violation operators in the 2HDM is given by [7]

$$d_n = (e\zeta_n^u\delta_u + e\zeta_n^d\delta_d) + (e\tilde{\zeta}_n^u\tilde{\delta}_u + e\tilde{\zeta}_n^d\tilde{\delta}_d) + \beta_n^G C_{\tilde{G}}, \tag{61}$$

where we have set $\Lambda = v$ as indicated earlier and the central values [7] for the hadronic matrix elements are

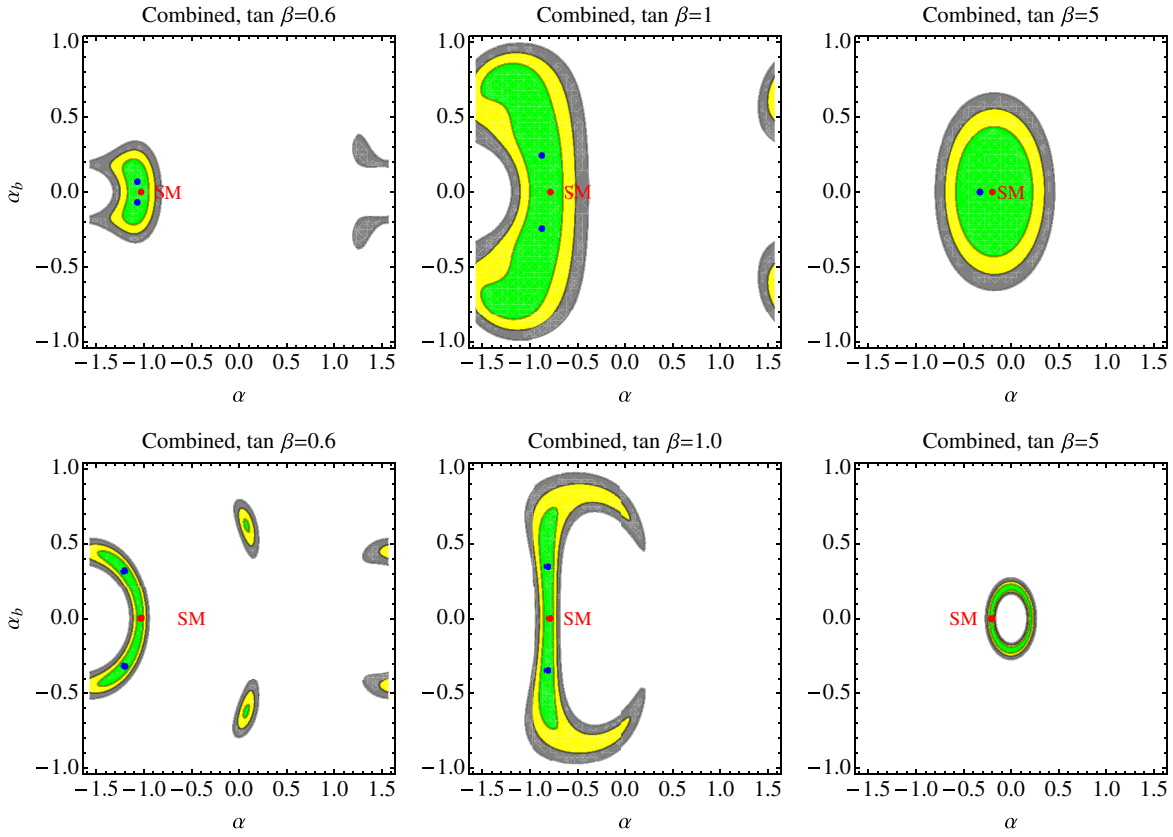

FIG. 4 (color online). Global fit to the LHC Higgs data on the event rates given in Table I, for different values of $\tan\beta$. (First row) Type I model. (Second row) Type II model. The other parameters are chosen to be $\alpha_c = 0.05$, $m_{H^+} = 420$ GeV, $m_{h_2} = 400$ GeV and $m_{h_3} = 450$ GeV. The 1, 2, and 3σ regions are in green, yellow, and gray, and the best-fit points are in blue.

$\zeta_n^u = 0.82 \times 10^{-8}$, $\zeta_n^d = -3.3 \times 10^{-8}$, $\tilde{\zeta}_n^u = 0.82 \times 10^{-8}$, $\zeta_n^d = 1.63 \times 10^{-8}$, and $\beta_n^G = 2 \times 10^{-20}$ e cm. The experimental upper bound on neutron EDM is [35]

$$d_n < 2.9 \times 10^{-26}\ e\,\text{cm}. \tag{62}$$

3. Diamagnetic atom EDMs

At present, the most stringent EDM limit has been obtained on the ^{199}Hg atom (see below). Efforts are under way to increase the sensitivity of this EDM search, while other groups are pursuing searches for the EDMs of other diamagnetic atoms, including ^{225}Ra and ^{129}Xe (for a discussion, see, e.g., Ref. [12]). To follow, we will consider the present ^{199}Hg constraint, as well as the prospective impact of future ^{199}Hg and ^{225}Ra searches. Diamagnetic atom EDMs arise primarily from their nuclear Schiff moments and a tensor semileptonic interaction. In the 2HDMs, the latter is suppressed by the same light fermion Yukawa factors that suppress $C_S^{(0)}$. The Schiff moment is generated by long-range, pion-exchange mediated P- and T-violating nucleon-nucleon interactions, where one vertex involves the P- and T-conserving strong πNN coupling and the second consists of TVPV interaction

$$\mathcal{L}_{\pi NN}^{\text{TVPV}} = \bar{N}[\bar{g}_\pi^{(0)}\vec{\tau}\cdot\vec{\pi} + \bar{g}_\pi^{(1)}\pi^0 + \bar{g}_\pi^{(2)}(2\tau_3\pi^0 - \vec{\tau}\cdot\vec{\pi})]N, \tag{63}$$

where the terms on the right-hand side correspond to isoscalar, isovector, and isotensor channels, respectively. In general, the isotensor coupling $\bar{g}_\pi^{(2)}$ is suppressed with respect to the other two [7], so we include only the latter in our analysis. Denoting the nuclear Schiff moment as S, one has [7]

$$d_{\text{Hg}} = \kappa_S S \approx \kappa_S \frac{2 m_N g_A}{F_\pi}(a_0 \bar{g}_\pi^{(0)} + a_1 \bar{g}_\pi^{(1)}), \tag{64}$$

where $g_A \approx 1.26$ and $F_\pi = 186$ MeV. For ^{199}Hg, we take the central values for the nuclear matrix elements from Ref. [7] ($a_0 = 0.01\ e\,\text{fm}^3$ and $a_1 = \pm 0.02\ e\,\text{fm}^3$), while the atomic sensitivity coefficient is $\kappa_S = -2.8 \times 10^{-4}$ fm^{-2} [36].[4] For radium, the central values are $a_0 = -1.5\ e\,\text{fm}^3$, $a_1 = 6.0\ e\,\text{fm}^3$, and $\kappa_S = -8.5 \times 10^{-4}$ fm^{-2} [36].

At the hadronic level, the TVPV coefficients $\bar{g}_\pi^{(0,1)}$ arise from quark CEDMs and the Weinberg operators [7]

[4]We note that Eq. (5.181) of Ref. [21] omitted the minus sign on this value of κ_S.

$$\bar{g}_\pi^{(0)} = \tilde{\eta}_{(0)}(\tilde{\delta}_u^G + \tilde{\delta}_d^G) + \gamma_{(0)}^{\tilde{G}} C_{\tilde{G}},$$
$$\bar{g}_\pi^{(1)} = \tilde{\eta}_{(1)}(\tilde{\delta}_u^G - \tilde{\delta}_d^G) + \gamma_{(1)}^{\tilde{G}} C_{\tilde{G}}, \quad (65)$$

where the hadronic matrix elements are $\tilde{\eta}_{(0)} = -2 \times 10^{-7}$, $\tilde{\eta}_{(1)} = -4 \times 10^{-7}$, and $\gamma_{(0)}^{\tilde{G}} \approx \gamma_{(1)}^{\tilde{G}} = 2 \times 10^{-6}$. There is also a contribution to $\bar{g}_\pi^{(i)}$ from the parity-violating four-quark operators, which we find to be unimportant for the 2HDMs here.

The current experimental upper bound on mercury EDM is [37]

$$d_{\rm Hg} < 3.1 \times 10^{-29}\ e\,{\rm cm}, \quad (66)$$

and we will use a conservative future sensitivity for the radium EDM [12]

$$d_{\rm Ra} < 10^{-27}\ e\,{\rm cm}. \quad (67)$$

IV. RESULTS

A. LHC Higgs data constraint

We perform a global fit to the Higgs data given in Table I, where all the measured event rates are normalized to the SM predictions and are of the form $\mu_f \pm \sigma_f$. The employed χ^2 is defined as

$$\chi^2 = \sum_f \frac{[\sigma_{h_1} {\rm Br}_{h_1\to f}/(\sigma_{h_1}^{\rm SM} {\rm Br}_{h_1\to f}^{\rm SM}) - \mu_f]^2}{\sigma_f^2}, \quad (68)$$

where the sum goes through all the Higgs decay channels. The results are shown in Fig. 4 in the two-dimensional $\alpha_b - \alpha$ plane, for fixed values of $\tan\beta = 0.6$, 1, and 5, respectively. The 1, 2, and 3σ regions are in green, yellow, and gray, and the blue points represent where the best fit is found.

Clearly, the SM limit always gives a good fit, well within 1σ. However, we find that for low values of $\tan\beta \lesssim 1$, nonzero CP violation is preferred over the SM. This is mainly driven by the excess in the diphoton channel which still persists at ATLAS. We also find when $\tan\beta \sim 1$ and $\alpha \approx \beta - \pi/2$, the largest possible α_b is allowed. In this case, the Higgs couplings defined in Eq. (15) are $|c_t| \approx |c_b| \approx |a| \approx \cos\alpha_b$ and $|\tilde{c}_t| \approx |\tilde{c}_b| \approx \sin\alpha_b$. The resulting χ^2 is a function of $\cos^2\alpha_b$, which, when $\alpha_b \to 0$, approaches $\chi^2_{\rm SM}$ for the SM case. Because the cosine function is rather "flat" around the origin, there is substantial room for α_b to deviate from zero, while $\chi^2 - \chi^2_{\rm SM}$ still remains small. The physical effect of nonzero CP violation is to enhance the rate for $h_1 \to \gamma\gamma$ and suppress the rate for the Vbb channel. At the same time, the Higgs total width is also slightly reduced. At large $\tan\beta$, we find the effects of CP violation are being enhanced; thus, the good fit region shrinks with the increasing $\tan\beta$. These facts suggest that the best place to look for a sizable possible CP violation angle is when $\tan\beta \approx 1$.

As indicated by Fig. 4, the LHC Higgs data imply strong constraints on the CP conserving angle α, while the constraints on the CP-violating angle α_b are generally relatively weaker. As we discuss below, EDM searches are more sensitive to the nonzero α_b, but less sensitive to α. In short, the Higgs studies and EDM searches provide complementary probes of the type I and type II 2HDMs.

B. Electron EDM constraint

Drawing on the Wilson coefficients computed in Appendix A; the hadronic, nuclear, and atomic computations summarized in Sec. III C; and the present and prospective EDM search sensitivities, we present numerical results for the EDM constraints on the CP violation parameter space. We give resulting constraints in the $\tan\beta$ vs. $\sin\alpha_b$ (Fig. 6), as well as a breakdown, or anatomy, of the various contributions and their RG evolution as a function of $\tan\beta$ (Figs. 5, 7, 8, and 9). We also discuss the implications of the constraints for the 2HDMs and the impact of the various hadronic and nuclear uncertainties.

We first consider the electron EDM, whose current limit is set by the ACME Collaboration, $d_e < 10.25 \times 10^{-29}\ e\,{\rm cm}$ at 95% confidence level. Strictly speaking, ACME sets a bound on the linear combination of d_e and a CP-odd four-fermion operator [see Eq. (60)]. In practice, we note the four-fermion contribution is always subdominant in the flavor conserving 2HDMs.

In Fig. 5, we plot the anatomy of various contributions [see Eq. (A12) in the Appendix] to the electron EDM as functions of $\tan\beta$. Here we have fixed the CP violation angle $\alpha_b = 0.7 \times 10^{-2}$ and have then determined α_c using Eq. (43). We note that the two solutions $\alpha_c^\pm$ give very similar plots. We fix the other parameters to be $m_{H^+} = 420$ GeV, $m_{h_2} = 400$ GeV, $m_{h_3} = 450$ GeV, $\nu = 1.0$, and $\alpha = \beta - \pi/2$.[5,6,7] We find the dominant contributions are always from $h\gamma\gamma$ or $H\gamma\gamma$ ($H = h_2$, h_3) diagrams at low or high $\tan\beta$ regimes, respectively. Around $\tan\beta \approx 10$–20, they have comparable magnitudes and opposite signs, leading to a cancellation in the total d_e. This cancellation leads to a sign change in d_e, but since we

[5]We have ensured that our choice of masses is consistent with constraints from electroweak oblique parameters. General expressions for oblique parameters in 2HDM were given by Grimus *et al.* [38].

[6]The charged Higgs mass is chosen to be > 380 GeV in order to satisfy $B \to X_s\gamma$ bounds [39].

[7]We note that the reported 3.4σ deviation of the rate for $\bar{B} \to D^{(*)}\tau^-\bar{\nu}_\tau$ [40] from the SM prediction cannot be accommodated by the 2HDM scenario analyzed here. For the parameter space that we consider, the discrepancy does not increase, though introduction of additional interactions would be needed to account for the difference. A study of the possibilities goes beyond the scope of the present study.

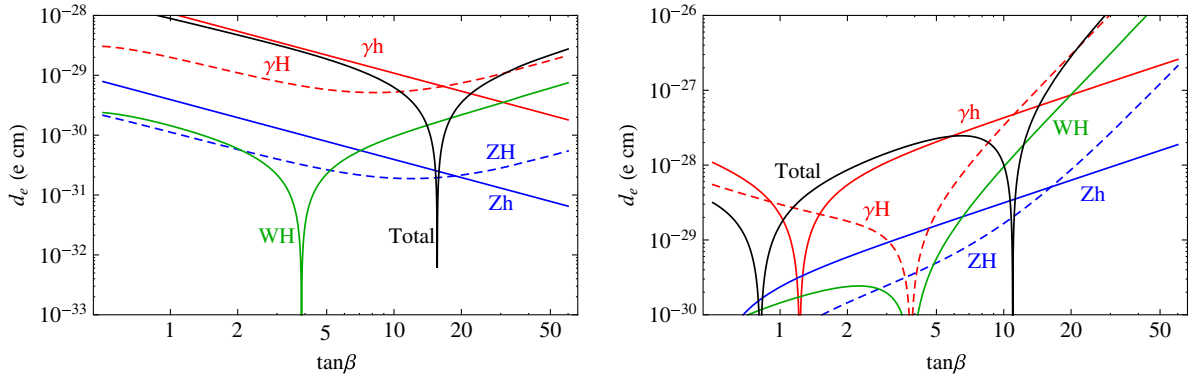

FIG. 5 (color online). The anatomy of various contributions to the electron EDM in flavor conserving 2HDMs. (Left panel) Type I model. (Right panel) Type II model. We plot the absolute values, so the dip in the curves implies a sign change. Parameters are chosen to be $\alpha = \beta - \pi/2$, $\alpha_b = 0.7 \times 10^{-2}$, $m_{H^+} = 420$ GeV, $m_{h_2} = 400$ GeV, $m_{h_3} = 450$ GeV, and $\nu = 1.0$. The parameter α_c is not independent and is obtained using Eq. (43), and we note that the two solutions $\alpha_c^{\pm}$ give very similar results here.

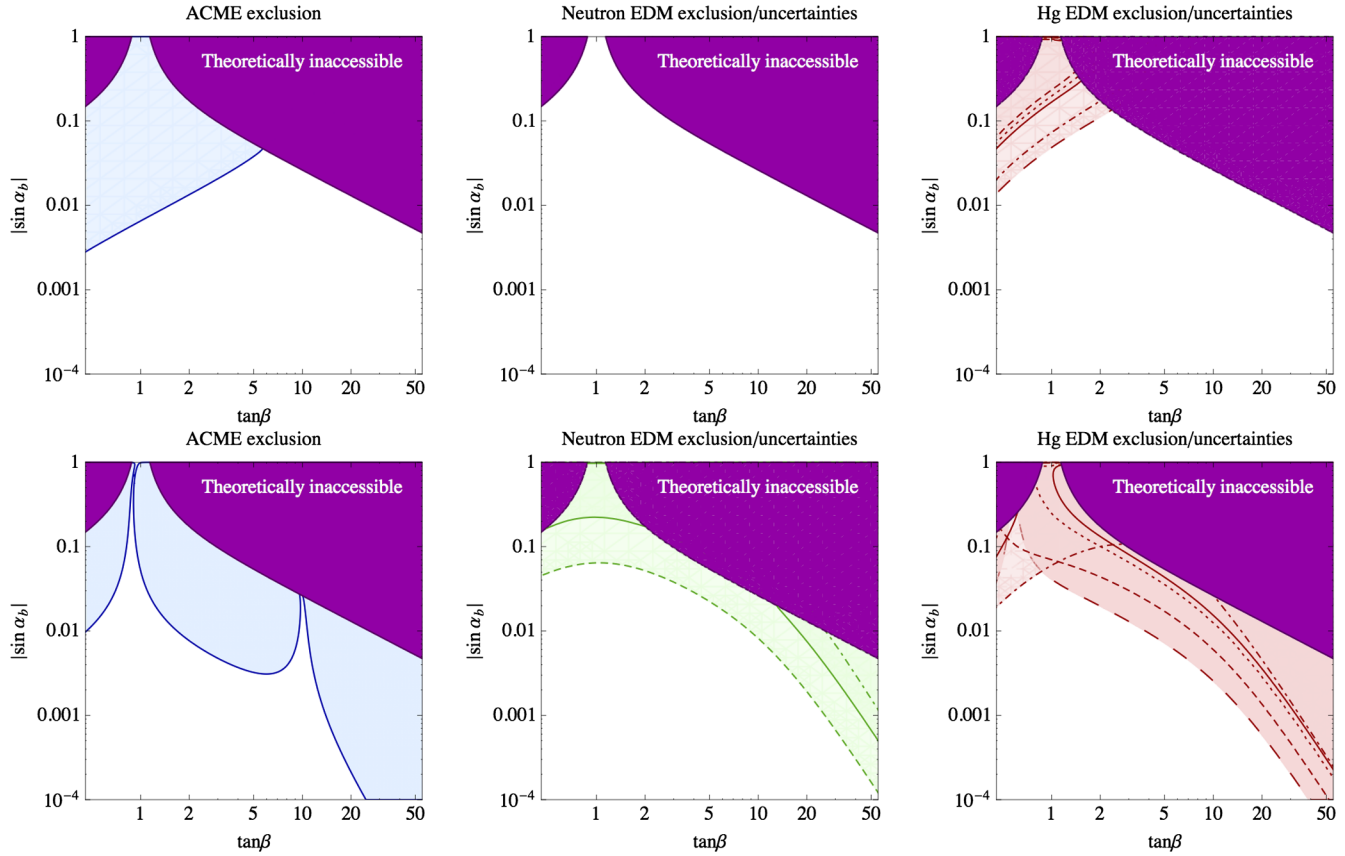

FIG. 6 (color online). Current constraints from the electron EDM (left panels), neutron EDM (middle panels) and ^{199}Hg EDM (right panels). (First row) Type I model. (Second row) Type II model. In all plots, we have imposed the condition that $\alpha = \beta - \pi/2$. The other parameters are chosen to be $m_{H^+} = 420$ GeV, $m_{h_2} = 400$ GeV, $m_{h_3} = 450$ GeV, and $\nu = 1.0$. Again, α_c is a dependent parameter solved using Eq. (43). The purple region is theoretically not accessible, because Eq. (43) does not have a real solution. For the neutron and mercury EDMs, theoretical uncertainties from hadronic and nuclear matrix elements are reflected by different curves. For the neutron EDM, we vary one of the most important hadronic matrix elements: $\tilde{\zeta}_n^d = 1.63 \times 10^{-8}$ (solid, central value), 0.4×10^{-8} (dot dashed), and 4.0×10^{-8} (dashed). For the mercury EDM, we take different sets of nuclear matrix element values: $a_0 = 0.01$, $a_1 = 0.02$ (solid, central value), $a_0 = 0.01$, $a_1 = 0.09$ (long dashed), $a_0 = 0.01$, $a_1 = -0.03$ (dashed), $a_0 = 0.005$, $a_1 = 0.02$ (dotted), and $a_0 = 0.05$, $a_1 = 0.02$ (dot dashed).

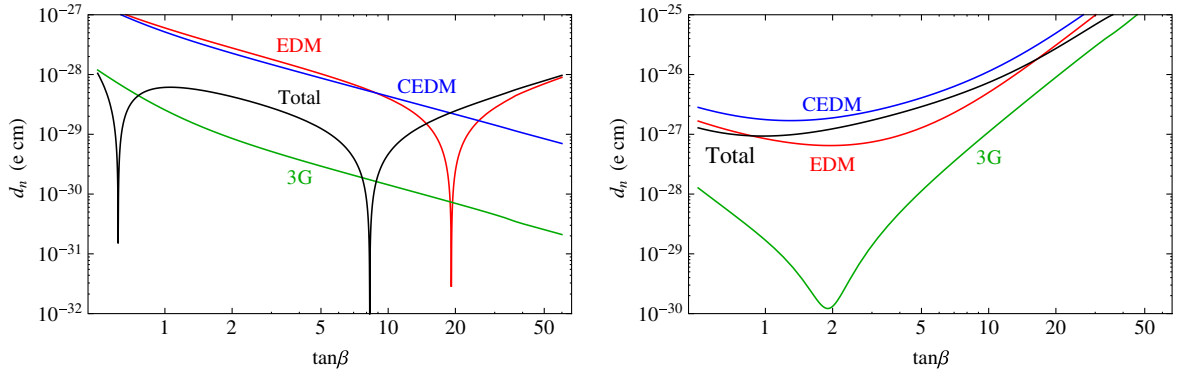

FIG. 7 (color online). The anatomy of various contributions to the neutron EDM in flavor conserving 2HDMs. (Left panel) Type I model. (Right panel) Type II model. We plot the absolute values, so the dip in the curves implies a sign change. The model parameters used are the same as in Fig. 5.

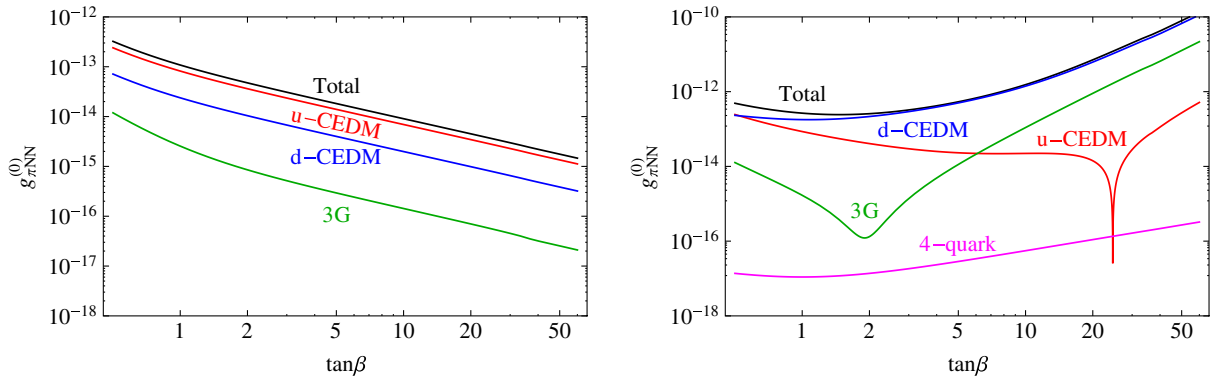

FIG. 8 (color online). The anatomy of various contributions to the $\bar{g}^{(0)}_{\pi NN}$ for atomic EDMs in flavor conserving 2HDMs. (Left panel) Type I model. (Right panel) Type II model. We plot the absolute values, so the dip in the curves implies a sign change. The model parameters used are the same as in Fig. 5.

plot $|d_e|$ it appears as a spike going toward zero. The $H^{\pm}W^{\mp}\gamma$ contribution can give corrections as large as 20% at large $\tan\beta$. The $hZ\gamma$ or $HZ\gamma$ contribution is always subdominant, because it is accidentally suppressed by the small Zee vector coupling, proportional to $(1-4\sin^2\theta_W)$.

The first column of Fig. 6 shows the ACME experimental constraint, where the blue region is excluded. Here, in order to compare with the fit to LHC Higgs data results in Fig. 4, we have made the plots in the $\sin\alpha_b$–$\tan\beta$ plane. Again, for a given $\alpha_b = 0.7\times10^{-2}$, there are two solutions for α_c from Eq. (43): $\alpha_c^{\pm}$. We find that all the EDM constraints for both choices give very similar results. For the type II 2HDM, there are two cancellation regions in $\tan\beta$. The one near $\tan\beta\sim1$ was recently noticed in Ref. [4,41], which is due to the cancellation between the top quark and the W loop in the $h\gamma\gamma$ type diagrams. The second region is near $\tan\beta\approx10$–20, due to the cancellation resulting from the $h\gamma\gamma$ and $H\gamma\gamma$ contributions. As we will show below, these cancellation regions can be closed when the neutron and mercury EDM limits are taken into account. A generic feature is that, for growing $\tan\beta$, the EDM constraints become weaker in the type I 2HDM but stronger in the type II 2HDM, which can be understood from the $\tan\beta$ dependencies in Eq. (27).

C. Ineffectiveness of a light-Higgs-only theory

From the discussion of electron EDM, we have learned that the heavy Higgs contributions via $H\gamma\gamma$ and $H^{\pm}W^{\mp}\gamma$ diagrams make non-negligible contributions to the total EDM. They can even be dominant at large $\tan\beta\gtrsim20$. This example illustrates the ineffectiveness of the "light Higgs effective theory," often performed as model independent analyses, which include the *CP* violation effects only from the lightest Higgs (a mass of 125 GeV). The key point is that a *CP*-violating Higgs sector usually contains more than one scalar at the electroweak scale, and all of them have *CP* violation interactions (in general). The total contribution therefore includes *CP* violation effects from not only *CP* even-odd neutral scalar mixings, but also the *CP* violation neutral-charged scalar interactions from the Higgs potential. This is necessarily model dependent. In this work, we

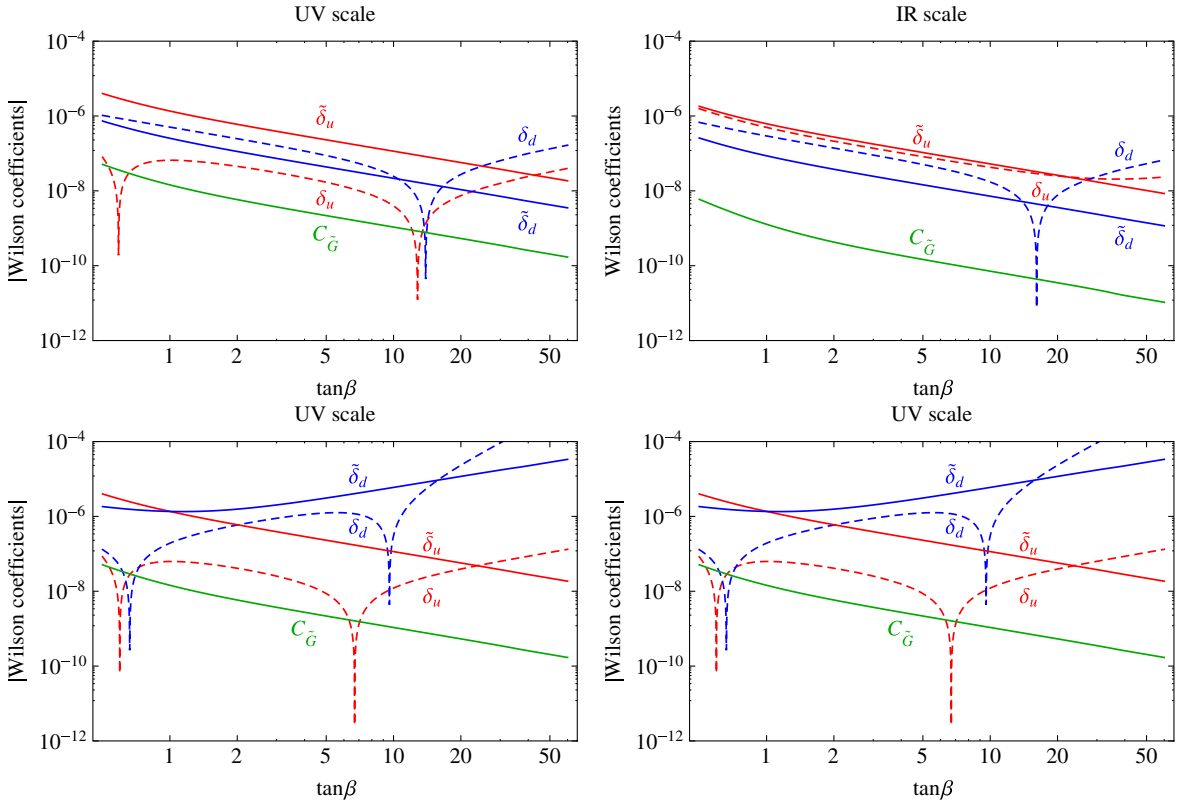

FIG. 9 (color online). The Wilson coefficients at the 2HDM scale (left column) and the GeV scale (right column). (First row) Type I model. (Second row) Type II model. We plot the absolute values, so the dip in the curves implies a sign change. The differences reflect the effects of leading-order QCD corrections in the RG running. The model parameters used are the same as in Fig. 5.

have included the complete contributions to EDMs in the flavor conserving (type I and type II) 2HDMs.

D. Neutron EDM constraint

Next, we consider the neutron EDM, whose current bound is $|d_n| < 2.9 \times 10^{-26}\ e\,\mathrm{cm}$. In Fig. 7, we plot the anatomy of neutron EDM, this time in terms of the various dimension-six operator contributions. The parameters are fixed as in Fig. 5, and the contributions to neutron EDM from light quark EDMs, CEDMs, and the Weinberg three-gluon operator are shown as functions of $\tan\beta$. The plot shows that in the type II model, the quark CEDM contributions to neutron EDM are larger than those from quark EDMs. In type I, these two contributions are similar in size. In both cases, the effect of the Weinberg operator is smaller. Also, in both types, EDM and CEDM contributions have the opposite sign, and total neutron EDM tends to be suppressed as a result. However, these statements depend on the hadronic matrix elements being close to their current best value.

The second column of Fig. 6 shows the bounds in the $\sin\alpha_b$–$\tan\beta$ plane. The green regions are excluded for three different choices of the hadronic matrix elements. Specifically, the down quark CEDM matrix element $\tilde{\zeta}_n^d$ takes the values 1.63×10^{-8} (solid), 0.4×10^{-8} (dot dashed), and 4.0×10^{-8} (dashed). This matrix element has a large impact, because the down quark CEDM is the largest Wilson coefficient for most values of $\tan\beta$. In the type II model and the most sensitive case with the largest matrix element $\tilde{\zeta}_n^d = 4.0 \times 10^{-8}$, α_b is constrained to be of order 0.1 or smaller. In the least sensitive case ($\tilde{\zeta}_n^d = 0.4 \times 10^{-8}$), no part of the $\sin\alpha_b$–$\tan\beta$ plane is excluded (with $\alpha = \beta - \pi/2$). The neutron EDM constraint is quite weak in the type I model, due to the near-total cancellation of the quark EDM and CEDM contributions.[8]

E. Mercury EDM constraint

We now come to the ^{199}Hg EDM limit of $|d_{Hg}| < 3.1 \times 10^{-29}\ e\,\mathrm{cm}$. The anatomy of the isoscalar πNN coupling $\bar{g}^{(0)}_{\pi NN}$ is shown in Fig. 8. Parameters are chosen as in Figs. 5 and 7, and contributions from the up and down CEDM Weinberg operator are plotted as functions of $\tan\beta$. The four-quark operator involving the up and down quarks also adds to $g^{(0)}_{\pi NN}$, but this effect is negligible, as shown in the type II plot. In the type I model, this effect is even smaller. The down quark CEDM gives the largest contribution to the πNN coupling in the type II model, but

[8]This cancellation depends crucially on the relative signs of the hadronic matrix elements; see below.

the Weinberg operator can be important for large $\tan\beta$. In type I, the up CEDM consistently makes up the largest bulk of $g_{\pi NN}^{(0)}$.

The parameter space excluded by the ^{199}Hg result is plotted in the right column of Fig. 6. As for the eEDM and nEDM plots, α is assumed to have the SM value of $\beta - \pi/2$. The general shape of the excluded region is similar to that in the other two experiments, with the weakest limits on α_b near $\tan\beta = 1$. As in the neutron case, our limits depend heavily on the value of hadronic and nuclear matrix elements. For illustration, several choices of the nuclear matrix elements a_0 and a_1 are shown. The current best values of $a_0 = 0.01\ e\,\mathrm{fm}^3$ and $a_1 = 0.02\ e\,\mathrm{fm}^3$ are represented by the solid line. In general, larger absolute values for the matrix elements imply stronger bounds, as expected, and the locations of cancellation regions are sensitive to the ratio between a_0 and a_1. In the more sensitive cases, α_b can be constrained to 0.1 or smaller at all values of $\tan\beta$.

F. Hadronic and nuclear uncertainties

We have noted in the discussion of neutron and ^{199}Hg constraints the effects of hadronic and nuclear matrix elements. Currently, calculations of these matrix elements are riddled with large uncertainties [7]. For the magnitudes of the matrix elements, there is guidance from naive dimensional analysis, which takes into account the chiral structures of the operators in question. However, the precise value of matrix elements involving quark CEDMs and the Weinberg three-gluon operator are only known to about an order of magnitude, and dimensional analysis does not tell us the signs of the matrix elements. We highlight two places where these uncertainties can change our results.

(i) In Figs. 7 and 8, we see that the Weinberg three-gluon operator is always subdominant as a contribution to the neutron and mercury EDMs. It is possible, though, that the actual matrix element may be an order of magnitude larger than the current best value. Then, the Weinberg operator would make the largest contribution to the neutron and mercury EDMs at large $\tan\beta$ in the type II model.

(ii) In the left panel of Fig. 7, the quark EDM and CEDM contributions to nEDM in the type I model are shown to be nearly equal, but with opposite signs, suppressing the total neutron EDM in the type I model. If the overall sign of the CEDM matrix element is opposite to that used here, the two effects would add constructively, making the neutron EDM limit much stronger.

In the absence of hadronic and nuclear matrix element uncertainties, improvements in neutron and diamagnetic atom searches will make them competitive with the present ThO result when constraining *CP* violation in 2HDM. At present, however, theoretical uncertainties are significant, making it difficult to draw firm quantitative conclusions regarding the impact of the present and prospective neutron and diamagnetic EDM results.

G. QCD running

Figure 9 illustrates the differences in the Wilson coefficients between the UV (weak) scale and the IR (hadronic) scale. For the type I model (top panels), there is no dramatic difference between the magnitude of the coefficients other than a slight enhancement in quark EDMs and CEDMs. For the type II model (bottom panels), however, there is a significant difference in the $\tan\beta$ dependence and the relative magnitudes of the coefficients. Part of this difference is explained by diagrams involving b quarks, which is not yet integrated out at the UV scale. Specifically, many of the growing behaviors at large $\tan\beta$ for the d-quark CEDM and the Weinberg operator are accounted for by simply adding the b-quark diagrams. However, the growth of the u-quark EDM and the u-quark CEDM at large $\tan\beta$ and the similarity of EDM and CEDM for each quark at all values of $\tan\beta$ are mainly due to the operator mixing in QCD. For this reason, we observe that QCD running must be taken into account when making quantitative claims about hadronic sources of *CP* violation.

H. Combined EDM constraints: Present and future

We summarize the combined EDM constraints of the electron (blue region), neutron (green), ^{199}Hg (red), and ^{225}Ra (yellow) in Fig. 10. For the neutron and atomic EDMs, we use the central values for the hadronic and nuclear matrix elements. The first column shows the present constraints. We find that the bound on electron EDM from the ACME experiment is presently by far the strongest, except for the cancellation region, which is closed by the mercury and neutron EDM bounds. The current constraints are, roughly, $\alpha_b, \alpha_c \lesssim 0.1$ for all $\tan\beta$ in type II 2HDM. For the type I model, the constraints are $\alpha_b \lesssim 0.1$, while α_c can still be of order 1 for $\tan\beta \gtrsim 5$. Therefore, it could be easier to search for *CP* violation effects related to the heavy scalars if they are discovered in future collider experiments.

The second column of Fig. 10 shows the future constraints if the neutron and mercury EDM experiments improve the current sensitivities by a factor of 10. We have also shown the future constraints in blue dashed curves if electron EDM is improved by another order of magnitude. The last column shows the situation when the neutron EDM limit is improved by a factor of 100, which is the goal for the experiment planned for the Fundamental Neutron Physics Beamline at the Oak Ridge National Laboratory Spallation Neutron Source. For the type II 2HDM, we find that the future neutron EDM experiments can improve the current limit on the *CP* violation angles α_b and α_c by 1 order of magnitude. The radium EDM also has the prospect of giving a comparable limit.

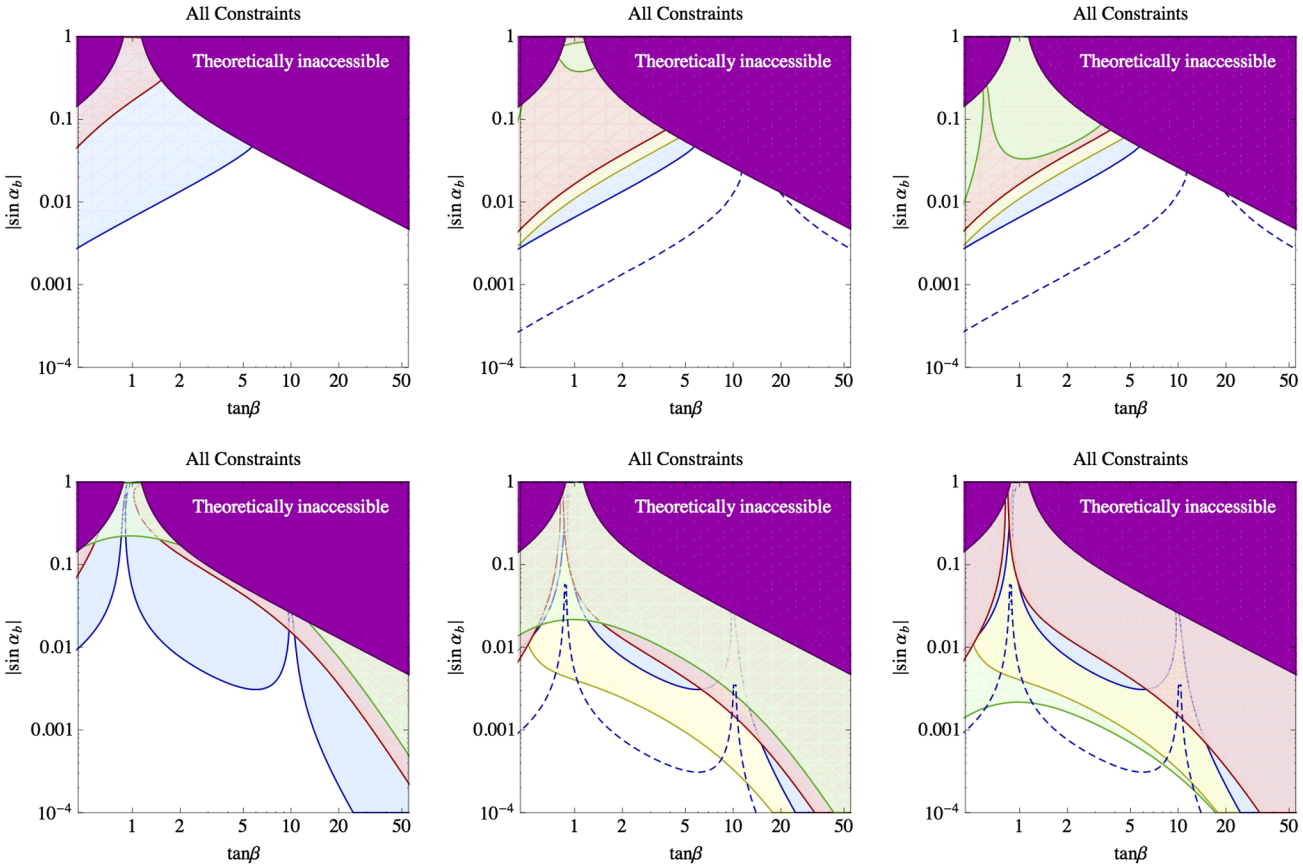

FIG. 10 (color online). Current and prospective future constraints from electron EDM (blue), neutron EDM (green), mercury EDM (red), and radium (yellow) in flavor conserving 2HDMs. (First row) Type I model. (Second row) Type II model. The model parameters used are the same as in Fig. 6. Central values of the hadronic and nuclear matrix elements are used. (Left column) Combined current limits. (Middle column) Combined future limits if the mercury and neutron EDMs are both improved by 1 order of magnitude. Also shown are the future constraints if electron EDM is improved by another order of magnitude (in blue dashed curves). (Right column) Combined future limits if the mercury and neutron EDMs are improved by 1 and 2 orders of magnitude, respectively.

Finally, we comment on the effects of changing the masses of the heavy scalars. While we have only presented the results for the case when the extra scalars have masses of order ~400 GeV, we have performed the same analyses with different masses of up to ~500 GeV. The constraints on the CP violation angle α_b become slightly weaker with heavier new scalars, but we find that there is no qualitative difference to our conclusions.

V. SUMMARY

The nature of CP violation beyond the Standard Model remains a question at the forefront of fundamental physics. The cosmic matter-antimatter asymmetry strongly implies that such a BSM CP violation should exist, but the associated mass scale and dynamics remain unknown. With the observation of the 125 GeV boson at the LHC, it is particularly interesting to ask whether the scalar sector of the larger framework containing the SM admits new sources of CP violation and, if so, whether their effects are experimentally accessible. In this study, we have explored this question in the context of flavor conserving 2HDMs, allowing for a new source of CP violation in the scalar potential. The present constraints on this type of CP violation are generally weaker than for scenarios where the BSM directly enters the couplings to SM fermions, as the associated contributions to electric dipole moments generically first appear at two-loop order. In this context, we find that present EDM limits are complementary to scalar sector constraints from LHC results, as the latter generally constrain the CP-conserving sector of the type I and type II models, whereas EDMs probe the CP violation parameter space. Moreover, despite the additional loop suppression, the present ThO, ^{199}Hg, and neutron EDM search constraints are quite severe, limiting $|\sin\alpha_b|$ to ~0.01 or smaller for most values of $\tan\beta$.

The next generation of EDM searches could extend the present reach by an order of magnitude or more and could allow one to distinguish between the type I and type II models. In particular, a nonzero neutron or diamagnetic atom EDM result would likely point to the type II model, as even the present ThO limit precludes an observable effect

in the type I scenario, given the planned sensitivity of the neutron and diamagnetic atom searches. Furthermore, it appears that a combination of searches using different systems would be needed to achieve a comprehensive probe of the relevant parameter space in the type II model. We emphasize, however, that these expectations are somewhat provisional, given the present substantial uncertainties associated with computations of the hadronic and nuclear matrix elements that we have quantified in this study. Achieving more robust computations would be particularly welcome, especially given the role of neutron and diamagnetic atom EDM searches in probing the type II flavor conserving 2HDM.

ACKNOWLEDGMENTS

We thank J. DeVries and W. Dekens for their helpful discussion of the effective operator anomalous dimension matrix. This work is partially supported by the Gordon and Betty Moore Foundation through Grant No. 776 to the Caltech Moore Center for Theoretical Cosmology and Physics and by U.S. DOE Grants No. DE-FG02-92ER40701 (Y. Z.) and No. DE-SC0011095 (S. I. and M. J. R-M.). The work of Y. Z. is also supported by a U.S. DOE Early Career Award under Grant No. DE-SC0010255.

APPENDIX A: WILSON COEFFICIENTS OF P- AND T-ODD OPERATORS AT THE 2HDM SCALE

In this appendix, we give the results of all the Wilson coefficients by integrating out the heavy particles at the 2HDM scale, $\Lambda \sim M_Z$. At this scale, the bottom quark is still light, and we discuss the matching conditions at the m_b scale in Sec. III B. The total contributions to the Weinberg, CEDM, and EDM operators are Eqs. (A1), (A2), and (A12), respectively.

1. Two-loop Weinberg operator

From Ref. [42], the contribution to the $d = 6$ Weinberg operator arises from the top loop, as shown in the left panel of Fig. 11, which gives

$$C_{\tilde{G}}(\Lambda) \equiv (C_{\tilde{G}})_t = -\frac{g_s^2}{3}\frac{1}{128\pi^4}\sum_{i=1}^{3} h_0(m_t/m_{h_i}) c_{t,i}\tilde{c}_{t,i}, \quad \text{(A1)}$$

where the function $h_0(x)$ can be found in Appendix B.

2. Two-loop Barr-Zee type contributions to CEDMs

For light fermions, the dominant contributions to their EDMs and CEDMs come from the two-loop Barr-Zee type diagrams [43], as shown in the middle and right panels of Fig. 11.

For the CEDM, the top quark in the upper (shaded) loop is first integrated out to obtain the $h_i GG$ or $h_i G\tilde{G}$ operators, which then contribute to the CEDM operators [44]

$$\tilde{\delta}_q(\Lambda) \equiv (\tilde{\delta}_q)_t^{hgg} = -g_s^2\frac{1}{128\pi^4}\sum_{i=1}^{3}[f(z_t^i)c_{t,i}\tilde{c}_{q,i} + g(z_t^i)\tilde{c}_{t,i}c_{q,i}], \quad \text{(A2)}$$

where $q = u,\ d,\ b$ and $z_t^i = m_{f_1}^2/m_{h_i}^2$. The two-loop functions $f(x)$ and $g(x)$ can be found in Appendix B.

3. Two-loop Barr-Zee type contributions to EDMs: Diagrams with $H^0\gamma\gamma$ and $H^0 Z\gamma$

The corresponding Barr-Zee type EDMs for light fermions are obtained with operator $h_i FF$ or $h_i F\tilde{F}$ from the upper (shaded) loop. See the right panel of Fig. 11. The contribution from the top quark is

$$(\delta_f)_t^{h\gamma\gamma} = -N_c Q_f Q_t^2 e^2 \frac{1}{64\pi^4} \times \sum_{i=1}^{3}[f(z_t^i)c_{t,i}\tilde{c}_{f,i} + g(z_t^i)\tilde{c}_{t,i}c_{f,i}]. \quad \text{(A3)}$$

Here, the external fermions relevant for our calculations are $f = u,\ d,\ e$. The analog contribution is to replace the photon propagator with that of the Z boson. It is worth noting that only the vector current of the $Z\bar{f}f$ coupling enters into the final EDM, which is

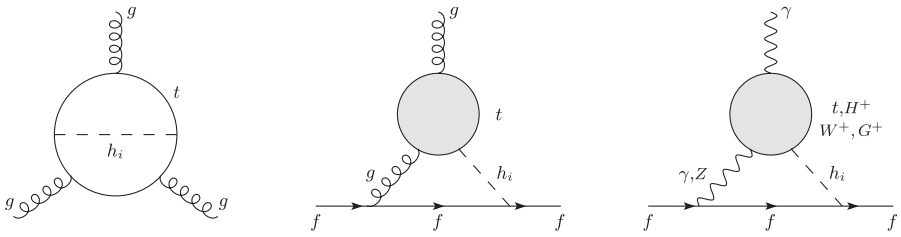

FIG. 11. (Left panel) Two-loop contribution to the Weinberg operator with *CP* violation neutral Higgs mixings. (Middle panel) Quark CEDM from Barr-Zee type diagrams with gh_i exchange and *CP* violation neutral Higgs mixings. The conjugate diagrams are not shown. (Right panel) Quark or lepton EDMs from Barr-Zee type diagrams with γh_i or Zh_i exchange and *CP* violation neutral Higgs mixings.

$$(\delta_f)_t^{hZ\gamma} = -N_c Q_{f_1} g^V_{Z\bar{f}f} g^V_{Z\bar{t}t} \frac{1}{64\pi^4} \sum_{i=1}^{3} [\tilde{f}(z_t^i, m_t^2/M_Z^2) c_{t,i} \tilde{c}_{f,i} + \tilde{g}(z_t^i, m_t^2/M_Z^2) \tilde{c}_{t,i} c_{f,i}], \tag{A4}$$

with $g^V_{f\bar{f}Z} = g(T_3^f - 2Q^f \sin^2\theta_W)/(2\cos\theta_W)$. The loop functions $\tilde{f}(z,x)$ and $\tilde{g}(z,x)$ can be found in Appendix B. The corresponding bottom quark loop contribution is properly taken into account in Sec. III B.

In the right panel of Fig. 11, the particles in the upper (shaded) loop can also be the W boson and its Goldstone boson. The gauge invariant contributions have been obtained in [45,46],

$$(\delta_f)_W^{h\gamma\gamma} = Q_f e^2 \frac{1}{256\pi^4} \sum_{i=1}^{3} \left[\left(6 + \frac{1}{z_w^i}\right) f(z_w^i) + \left(10 - \frac{1}{z_w^i}\right) g(z_w^i) \right] a_i \tilde{c}_{f,i}, \tag{A5}$$

$$(\delta_f)_W^{hZ\gamma} = g^V_{Z\bar{f}f} g_{ZWW} \frac{1}{256\pi^4} \sum_{i=1}^{3} \left[\left(6 - \sec^2\theta_W + \frac{2 - \sec^2\theta_W}{2z_w^i}\right) \tilde{f}(z_w^i, \cos^2\theta_W) + \left(10 - 3\sec^2\theta_W - \frac{2 - \sec^2\theta_W}{2z_w^i}\right) \tilde{g}(z_w^i, \cos^2\theta_W) \right] a_i \tilde{c}_{f_i}, \tag{A6}$$

where $z_w^i = M_W^2/m_{h_i}^2$ and $g_{WWZ}/e = \cot\theta_W$.

Similarly, the physical charged scalar can also run in the loop of Fig. 11. This is similar to the quark contribution discussed in the supersymmetric framework [47]. With the couplings defined in Eq. (30), its contributions to EDM are

$$(\delta_f)_{H^+}^{h\gamma\gamma} = Q_f e^2 \frac{1}{256\pi^4} \left(\frac{v}{m_{H^+}}\right)^2 \sum_{i=1}^{3} [f(z_H^i) - g(z_H^i)] \bar{\lambda}_i \tilde{c}_{f,i}, \tag{A7}$$

$$(\delta_f)_{H^+}^{hZ\gamma} = g^V_{Z\bar{f}f} g_{ZH^+H^-} \frac{1}{256\pi^4} \left(\frac{v}{m_{H^+}}\right)^2 \times \sum_{i=1}^{3} [\tilde{f}(z_H^i, m_{H^+}^2/M_Z^2) - \tilde{g}(z_H^i, m_{H^+}^2/M_Z^2)] \bar{\lambda}_i \tilde{c}_{f,i}, \tag{A8}$$

with $z_H^i = m_{H^+}^2/m_{h_1}^2$ and $g_{ZH^+H^-}/e = \cot\theta_W(1 - \tan^2\theta_W)/2$.

4. Two-loop Barr-Zee type contributions to EDMs: Diagrams with $H^\pm W^\mp \gamma$

The left panel of Fig. 12 represents the contribution where the upper loop yields an $H^\pm W^\mp \gamma$ operator. This contribution has not been included in the 2HDM calculations until very recently [46] (see [48] for the counterpart in supersymmetric models).

Here we would like to stress that it arises from the only source of CP violation in the Higgs potential. In the effective theory language, the possible gauge invariant operators for the upper (shaded) loop include

$$C_{ij} \phi_i^\dagger \frac{\sigma^a}{2} W^a_{\mu\nu} \phi_j B^{\mu\nu}, \qquad \tilde{C}_{ij} \phi_i^\dagger \frac{\sigma^a}{2} W^a_{\mu\nu} \phi_j \tilde{B}^{\mu\nu}, \tag{A9}$$

where C_{ij} and $\tilde{C}_{ij}$ are the Wilson coefficients. Because of the CP properties, fermion EDMs are proportional to the imaginary part of C_{ij} or the real part of $\tilde{C}_{ij}$. Here we argue that, in the flavor conserving 2HDMs discussed in this work, only the scalar loop could contribute to C_{12} and, eventually, to EDMs. A representative diagram is shown in the right panel of Fig. 12. It is proportional to

$$\mathrm{Im}(\lambda_5 m_{12}^{2*} v_1^* v_2) = -|\lambda_5 m_{12}^2 v_1 v_2| \sin\delta_2. \tag{A10}$$

Using the relation in Eq. (13), the above quantity is indeed related to the unique CP violation source in the model.

The fermionic loops do not contribute because the physical charge Higgs and quark couplings have the structure proportional to the corresponding CKM element. As a result, the coefficients C_{ij} are purely real and $\tilde{C}_{ij}$ are purely imaginary. They contribute to magnetic dipole moments instead of EDMs.

The gauge invariant contributions to EDMs from this class of diagrams have been calculated recently in [46]:

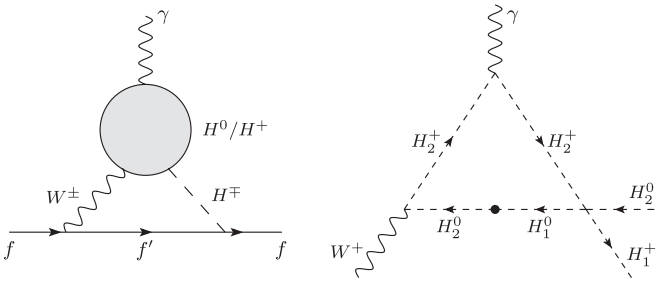

FIG. 12. (Left panel) Quark or lepton EDM from $W^\pm H^\mp$ exchange and CP violation Higgs interactions. (Right panel) A scalar loop contribution to the $\phi_1^\dagger \frac{\sigma^a}{2} W^a_{\mu\nu} \phi_2 B^{\mu\nu}$ effective operator, which then contributes to EDM as the upper loop of the left panel.

$$(\delta_f)_H^{HW\gamma} = \frac{1}{512\pi^4} s_f \sum_i \left[\frac{e^2}{2\sin^2\theta_W} \mathcal{I}_4(m_{h_i}^2, m_{H^+}^2) a_i \tilde{c}_{f,i} - \mathcal{I}_5(m_{h_i}^2, m_{H^+}^2) \bar{\lambda}_i \tilde{c}_{f,i} \right], \tag{A11}$$

where the functions $\mathcal{I}_{4,5}(m_1^2, m_2^2)$ are given in Appendix B. The coefficient $s_f = -1$ for up-type quarks and $s_f = +1$ for down-type quarks and charged leptons.

To summarize, the total contribution to fermion EDM is the sum of Eqs. (A3)–(A8) and (A11),

$$\begin{aligned}\delta_f(\Lambda) \equiv\ & (\delta_f)_t^{h\gamma\gamma} + (\delta_f)_t^{hZ\gamma} + (\delta_f)_W^{h\gamma\gamma} \\ & + (\delta_f)_W^{hZ\gamma} + (\delta_f)_{H^+}^{h\gamma\gamma} + (\delta_f)_{H^+}^{hZ\gamma} + (\delta_f)_H^{HW\gamma}. \end{aligned} \tag{A12}$$

APPENDIX B: LOOP FUNCTIONS

In this appendix, we collect all the loop functions used in previous sections:

$$h_0(z) = \frac{z^4}{2} \int_0^1 dx \int_0^1 dy \frac{x^3 y^3 (1-x)}{(z^2 x(1-xy) + (1-y)(1-x))^2}, \tag{B1}$$

$$f(z) = \frac{z}{2} \int_0^1 dx \frac{1-2x(1-x)}{x(1-x)-z} \log \frac{x(1-x)}{z}, \tag{B2}$$

$$g(z) = \frac{z}{2} \int_0^1 dx \frac{1}{x(1-x)-z} \log \frac{x(1-x)}{z}, \tag{B3}$$

$$\begin{aligned} h(z) = & \frac{z}{2} \int_0^1 dx \frac{1}{z - x(1-x)} \\ & \times \left(1 + \frac{z}{z - x(1-x)} \log \frac{x(1-x)}{z} \right), \end{aligned} \tag{B4}$$

$$\tilde{f}(x,y) = \frac{y f(x)}{y-x} + \frac{x f(y)}{x-y}, \tag{B5}$$

$$\tilde{g}(x,y) = \frac{y g(x)}{y-x} + \frac{x g(y)}{x-y}, \tag{B6}$$

$$\mathcal{I}_{4,5}(m_1^2, m_2^2) = \frac{M_W^2}{m_{H^+}^2 - M_W^2} (I_{4,5}(M_W^2, m_1^2) - I_{4,5}(m_2^2, m_1^2)), \tag{B7}$$

$$\begin{aligned} I_4(m_1^2, m_2^2) = & \int_0^1 dz (1-z)^2 \left(z - 4 + z \frac{m_{H^+}^2 - m_2^2}{M_W^2} \right) \\ & \times \frac{m_1^2}{M_W^2(1-z) + m_2^2 z - m_1^2 z(1-z)} \\ & \times \log \frac{M_W^2(1-z) + m_2^2 z}{m_1^2 z(1-z)}, \end{aligned} \tag{B8}$$

$$\begin{aligned} I_5(m_1^2, m_2^2) = & \int_0^1 dz \frac{m_1^2 z (1-z)^2}{M_W^2(1-z) + m_2^2 z - m_1^2 z(1-z)} \\ & \times \log \frac{M_W^2(1-z) + m_2^2 z}{m_1^2 z(1-z)}. \end{aligned} \tag{B9}$$

[1] J. F. Gunion, H. E. Haber, G. L. Kane, and S. Dawson, Front. Phys. **80**, 1 (2000).
[2] G. C. Branco, P. M. Ferreira, L. Lavoura, M. N. Rebelo, M. Sher, and J. P. Silva, Phys. Rep. **516**, 1 (2012).
[3] For a recent review, see D. E. Morrissey and M. J. Ramsey-Musolf, New J. Phys. **14**, 125003 (2012).
[4] J. Shu and Y. Zhang, Phys. Rev. Lett. **111**, 091801 (2013).
[5] L. Fromme, S. J. Huber, and M. Seniuch, J. High Energy Phys. 11 (2006) 038.
[6] C. Cheung and Y. Zhang, J. High Energy Phys. 09 (2013) 002.
[7] J. Engel, M. J. Ramsey-Musolf, and U. van Kolck, Prog. Part. Nucl. Phys. **71**, 21 (2013).
[8] T. Fukuyama, Int. J. Mod. Phys. A **27**, 1230015 (2012).
[9] M. Pospelov and A. Ritz, Ann. Phys. (Amsterdam) **318**, 119 (2005).
[10] W. Bernreuther and M. Suzuki, Rev. Mod. Phys. **63**, 313 (1991); **64**633(E) (1992).
[11] J. Baron *et al.* (ACME Collaboration), Science **343**, 269 (2014).
[12] K. Kumar, Z.-T. Lu, and M. J. Ramsey-Musolf, arXiv:1312.5416.
[13] S. L. Glashow and S. Weinberg, Phys. Rev. D **15**, 1958 (1977).
[14] A. J. Buras, G. Isidori, and P. Paradisi, Phys. Lett. B **694**, 402 (2011).
[15] J. M. Cline, K. Kainulainen, and M. Trott, J. High Energy Phys. 11 (2011) 089.
[16] M. Jung and A. Pich, J. High Energy Phys. 04 (2014) 076.

[17] E. Accomando, A. G. Akeroyd, E. Akhmetzyanova, J. Albert, A. Alves, N. Amapane, M. Aoki, G. Azuelos *et al.*, arXiv:hep-ph/0608079.
[18] B. Grzadkowski, O. M. Ogreid, and P. Osland, J. High Energy Phys. 01 (2014) 105.
[19] T. D. Lee, Phys. Rep. **9C**, 143 (1974).
[20] Y. B. Zeldovich, I. Y. Kobzarev, and L. B. Okun, Zh. Eksp. Teor. Fiz. **67**, 3 (1974) [Sov. Phys. JETP **40**, 1 (1974)].
[21] A. W. El Kaffas, P. Osland, and O. M. Ogreid, Phys. Rev. D **76**, 095001 (2007).
[22] T. Hayashi, Y. Koide, M. Matsuda, and M. Tanimoto, Prog. Theor. Phys. **91**, 915 (1994).
[23] H. E. Haber, G. L. Kane, and T. Sterling, Nucl. Phys. **B161**, 493 (1979).
[24] ATLAS Collaboration, Report No. ATLAS-CONF-2013-034.
[25] CMS Collaboration, Reports Nos. CMS-HIG-13-001, No. CMS-HIG-13-002, No. CMS-HIG-13-004; V. Dutta, *Proceedings of Moriond 2013*, https://indico.in2p3.fr/getFile.py/access?contribId=57&sessionId=6&resId=0&materialId=slides&confId=7411; G. Gomez-Ceballos, *Proceedings of Moriond 2013*, https://indico.in2p3.fr/getFile.py/access?contribId=16&sessionId=6&resId=0&materialId=slides&confId=7411.
[26] A. Freitas and P. Schwaller, Phys. Rev. D **87**, 055014 (2013).
[27] A. Celis, V. Ilisie, and A. Pich, J. High Energy Phys. 07 (2013) 053.
[28] A. Djouadi and G. Moreau, arXiv:1303.6591.
[29] W.-F. Chang, W.-P. Pan, and F. Xu, Phys. Rev. D **88**, 033004 (2013).
[30] W. Dekens and J. de Vries, J. High Energy Phys. 05 (2013) 149.
[31] J. Hisano, K. Tsumura, and M. J. S. Yang, Phys. Lett. B **713**, 473 (2012).
[32] G. Degrassi, E. Franco, S. Marchetti, and L. Silvestrini, J. High Energy Phys. 11 (2005) 044.
[33] V. D. Barger, A. K. Das, and C. Kao, Phys. Rev. D **55**, 7099 (1997).
[34] G. Boyd, A. K. Gupta, S. P. Trivedi, and M. B. Wise, Phys. Lett. B **241**, 584 (1990).
[35] C. A. Baker, D. D. Doyle, P. Geltenbort, K. Green, M. G. D. van der Grinten, P. G. Harris, P. Iaydjiev, S. N. Ivanov *et al.*, Phys. Rev. Lett. **97**, 131801 (2006).
[36] V. A. Dzuba, V. V. Flambaum, J. S. M. Ginges, and M. G. Kozlov, Phys. Rev. A **66**, 012111 (2002).
[37] W. C. Griffith, M. D. Swallows, T. H. Loftus, M. V. Romalis, B. R. Heckel, and E. N. Fortson, Phys. Rev. Lett. **102**, 101601 (2009).
[38] W. Grimus, L. Lavoura, O. M. Ogreid, and P. Osland, Nucl. Phys. **B801**, 81 (2008).
[39] T. Hermann, M. Misiak, and M. Steinhauser, J. High Energy Phys. 11 (2012) 036.
[40] J. P. Lees *et al.* (*BABAR* Collaboration), Phys. Rev. Lett. **109**, 101802 (2012).
[41] S. Ipek, Phys. Rev. D **89**, 073012 (2014).
[42] S. Weinberg, Phys. Rev. Lett. **63**, 2333 (1989); D. A. Dicus, Phys. Rev. D **41**, 999 (1990).
[43] S. M. Barr and A. Zee, Phys. Rev. Lett. **65**, 21 (1990); **65**, 2920(E) (1990).
[44] J. F. Gunion and D. Wyler, Phys. Lett. B **248**, 170 (1990).
[45] D. Chang, W.-Y. Keung, and T. C. Yuan, Phys. Rev. D **43**, R14 (1991).
[46] T. Abe, J. Hisano, T. Kitahara, and K. Tobioka, J. High Energy Phys. 01 (2014) 106.
[47] D. Chang, W.-Y. Keung, and A. Pilaftsis, Phys. Rev. Lett. **82**, 900 (1999); **83**3972(E) (1999).
[48] D. Chang, W.-F. Chang, and W.-Y. Keung, Phys. Lett. B **478**, 239 (2000); A. Pilaftsis, Phys. Lett. B **471**, 174 (1999).